Extended methods

Our reverse-engineering approach has three inter-dependent components (see also Fig. 2 of the main paper): (i) quantitative spatio-temporal gene expression data covering the trunk gap genes and their external regulatory inputs, (ii) the mathematical formulation of gene circuit models, and (iii) a global optimisation procedure to fit models and find gene circuit parameters that enable our model to faithfully reproduce the gene expression data. The main paper contains a general, high-level description. Here we elaborate on the details that are specific to the reverse-engineering of *M. abdita*.

Data acquisition and processing

Trunk gap genes: As described in (Crombach et al., 2012b), initially gap gene expression is normalized to values in the range $[0,1]$. We rescale these expression patterns such that the final gap gene expression levels mimick the accumulation of mRNA transcripts, peak around T3–T5, and then decline towards the end of the blastoderm stage (T6–T8). We slightly modified this post-processing protocol to adapt it to *M. abdita*: in this species, the retraction of the posterior *hb* domain from the pole of the embryo takes place over two time classes (T6 and T7; Wotton et al., 2015b), and involves gradual down-regulation of *hb* levels in the posterior-most region of the embryo. We capture this complex and transient retraction by introducing intermediate posterior boundaries that have a lower concentration bound of 0.667 at T6 and 0.333 at T7, instead of the default behaviour of assigning a 0.0 lower concentration bound. In this manner, the posterior *hb* boundary forms gradually over time, instead of near-instantly from one time class to the next.

External inputs: Trunk gap genes in both *M. abdita* and *D. melanogaster* are regulated by additional factors, which are implemented as external inputs (that are not themselves regulated) in our models: the maternal co-ordinate genes *bicoid* (*bcd*) and *caudal* (*cad*), and the terminal gap genes *tailless* (*tll*) and *huckebein* (*hkb*). Expression data for these factors are used as external inputs to gene regulation in our gene circuit models.

Ideally, these external inputs would consist of quantitative protein expression data. Unfortunately, over six years of consistent effort have failed to raise a functional antibody against *M. abdita* Bcd protein, which makes it impossible for us to measure protein concentrations directly. Therefore, we use an alternative approach to estimate protein gradients. The resulting approximated expression profiles for Bcd and Cad are shown in Figure S1.

In the case of Bcd, we assume a simple model where protein diffuses from an anteriorly localised source of mRNA (Grimm et al., 2010; Little et al., 2011; Stauber et al., 1999, 2002, 2000; Wotton et al., 2015b). This results in an approximately exponential steady-state distribution of Bcd protein along the A–P axis (Driever and Nüsslein-Volhard, 1988a,b; Gregor et al., 2007; Manu et al., 2009b; Surkova et al., 2008). The critical parameter that describes the scale of an exponential curve is the slope λ (Grimm et al., 2010). Since *M. abdita* Bcd is of similar size than the *D. melanogaster* protein, and shares extensive sequence similarity (Stauber et al., 1999), we assume that both proteins have comparable diffusive properties. Based on this, we first measure λ for *D. melanogaster* by fitting a single exponential curve $y = e^{-\lambda(x-a)}$ to Bcd protein expression data from the FlyEx database (http://urchin.spbcas.ru/flyex) (Pisarev et al., 2009; Poustelnikova et al., 2004). In this equation, y equals Bcd concentration, x A–P % position (where 0% is the anterior pole), and a represents the spatial extent of the mRNA source as described in more detail below. This fit yields $\lambda_{Dm} = 0.062$, which is the value used for our *D. melanogaster* models. We have previously shown that a time-invariant Bcd gradient, approximated as described here, yields modelling results which are equivalent to those obtained with models fit using measured Bcd protein data in *D. melanogaster* (Crombach et al., 2012b).

We then generated a series of plausible λ values for *M. abdita* around the measured value from *D. melanogaster*: $\lambda_{Ma} \in \{0.050, 0.060, 0.065, 0.070, 0.080\}$. Note that our definition of the scaling parameter implies that the greater λ, the faster the gradient decays along the A–P axis, and hence the shorter the gradient's scale. We established that our results are not affected by the precise choice of λ_{Ma}

(see Section). All *M. abdita* models presented in the main paper and our detailed regulatory analysis below use $\lambda_{Ma} = 0.065$.

Next, we considered the observed extent of the mRNA source. In *D. melanogaster*, >90% of mRNA is present in the anterior 20% of the embryo (Little et al., 2011), a result confirmed by our own *in situ* hybridisation measurements (Table S1). For *M. abdita*, we find a larger mRNA expression domain, extending to approximately 33% A–P position (Table S1; see also Stauber et al., 1999, 2002, 2000; Wotton et al., 2015b). We incorporate this difference in mRNA localisation by starting the *D. melanogaster* exponential curve at $a_{Dm} = 10\%$, and the *M. abdita* curve at $a_{Ma} = 16\%$ A–P position.

Finally, we consider gradient dynamics. In *D. melanogaster*, the Bcd gradient stays constant until time class T3 in cleavage cycle 14A, after which it decays linearly over time (Surkova et al., 2008) at a rate of 0.015 arbitrary concentration units per minute. In our models, we assume equivalent temporal behaviour for the Bcd gradient in *M. abdita*. Note that our time-variable approximation of Bcd in this paper differs from that in (Crombach et al., 2012b), which assumed Bcd to remain constant over time.

Expression profiles of Cad were approximated as follows. The main difference between *M. abdita* and *D. melanogaster* is that *cad* is not expressed maternally in the former, while zygotic expression profiles are remarkably similar in both species (Mlodzik and Gehring, 1987; Moreno and Morata, 1999; Schulz and Tautz, 1995; Stauber et al., 2008; Wotton et al., 2015b). We evaluated the onset of *cad* mRNA and protein expression as well as the position and width of the posterior stripe of late *cad* expression in *M. abdita* based on *in situ* hybridisation and antibody staining experiments (Wotton et al., 2015b, and data not shown): while *cad* mRNA is first detectable at the start of C11, we observe Cad protein appearing only in C12, with expression peaking at mid cycle C14A (T4). *cad* transcript and protein subsequently disappear from the abdominal region (T5–T8), and only a broad posterior stripe remains at the onset of gastrulation. In addition, Cad distribution is graded in the middle of the embryo, while it is consistently high in the posterior. Based on these considerations, a smooth approximation to the observed pattern was created using 2D thin-plate splines. Again, an equivalent approximation in *D. melanogaster* yields correct and accurate model fitting results compared to those based on direct measurements of the Cad protein profile (Crombach et al., 2012b).

For the terminal gap genes *tll* and *hkb*, we do not estimate the extent of protein expression domains. Instead, we use mRNA profiles interpolated between measured time points. Measurements of boundary positions were carried out as described for trunk gap genes above. We have previously established that such interpolated mRNA patterns yield fitted gap gene circuits which are equivalent to those obtained using protein expression profiles for terminal gap genes in *D. melanogaster* (Crombach et al., 2012b).

Gene circuits

In the gene circuit formalism, a fly embryo is represented as a one-dimensional array of nuclei along the A–P axis. This is justified by the fact that trunk gap gene regulation is exclusively happening along this axis (Jaeger, 2011). The trunk region is defined as 30–91% for *M. abdita*, and as 35–87% A–P position for *D. melanogaster*. This choice ensures compatibility with previous *D. melanogaster* models (Ashyraliyev et al., 2009; Crombach et al., 2012b), and the presence of an approximately equivalent set of gap gene expression domains in models for both species. In total, we have 16 nuclei in mitotic cycle C12, 31 in C13, and 61 in C14A for *M. abdita*. With four gap genes, this amounts to systems of 64, 124, and 244 ODEs, respectively. For *D. melanogaster*, we are dealing with systems of 108, and 212 ODEs in C13 and C14A, respectively.

Model fitting

Parallel Lam Simulated Annealing iteratively approximates the minimum of a cost function (see also Fig. 2B in main paper). This function associates a cost with every candidate solution (gene circuit with a specific set of parameters), by calculating the difference between model output and expression profiles in the data. We use a Weighted Least Squares (WLS) cost function—with artificial weights that are inversely proportional to expression levels (Crombach et al., 2012b)—to fit gene circuits to mRNA gap

gene expression data:

$$\text{cost} = \sum_{a \in G} \sum_{t \in T} \sum_{i \in N_c(n)} v_i^a(t) \left(g_i^a(t) - \text{data}_i^a(t) \right)^2 \tag{1}$$

with G the set of trunk gap genes as defined in the main paper, T the set of time points for which we have data (C12, C13, C14A: T1–T8), $N_c(n)$ the number of nuclei after n mitotic cycles, v_i^a weights, and $\text{data}_i^a(t)$ the mRNA expression level of gap gene a in nucleus i at time point t.

The above scoring function has the drawback that its value depends on the number of data points used for fitting. Therefore, we use a Root Mean Square (RMS) score to compare goodness of fit between series of optimisation runs using different data sets and in different species. The RMS score is defined as:

$$\text{RMS} = \sqrt{\frac{1}{N_{data}} \sum_{a \in G} \sum_{t \in T} \sum_{i \in N_c(n)} \left(g_i^a(t) - \text{data}_i^a(t) \right)^2} \tag{2}$$

with $N_{Ma} = 2140$ and $N_{Dm} = 1804$ the total number of data points in *M. abdita* and *D. melanogaster*, respectively. As a rule of thumb, mRNA-based gene circuits with RMS > 30.0 have expression defects that render them unsuitable for further analysis (see below).

Parameter search space was controlled by linear and non-linear constraints as described previously (Ashyraliyev et al., 2009; Crombach et al., 2012b; Jaeger et al., 2004a,b). In addition, we fixed a number of parameter values during optimisation: for both species E weights for the effect of Hkb on *Kr*, *kni*, and *gt* were set to zero, and for all gap genes h^a was set to -2.5. This improves parameter determinability without affecting the quality of the fits (see below, and Ashyraliyev et al., 2009).

A summary of interconnectivity matrices for scenarios with different *M. abdita* Bcd gradients is shown in Figure S2, with *D. melanogaster* matrices for both mRNA- and protein-based circuits shown for comparison in Figure S3. We discuss these scenarios in detail in Section below. Only the scenario with a λ_{Ma} of 0.065 was used for further analysis.

We did not perform practical (*a posteriori*) identifiability analysis for our *M. abdita* circuits. Previous results indicate that statistical parameter determinability is limited when using mRNA data for fitting in *D. melanogaster* (Crombach et al., 2012b). Being aware of this caveat, we argue that it is not a serious issue in practice. First, for most parameters, scatter plots of parameter values show a very clear trend towards specific types of interactions, which yields a clear consensus prediction of a specific regulatory structure (see Fig. 3 of the main paper and Section below). These predicted interactions can then be verified by comparing them to evidence from gene knock-down experiments using RNA interference (RNAi; see Section below). A close, quantitative match between model predictions and experimental evidence strongly suggests that our modelling results are specific, accurate, and biologically informative.

Selection of gene circuits for analysis

Only a subset of fitted gene circuits are deemed good enough to be selected for further analysis. After testing for numerical stability and discarding fits with an RMS > 30.0 (Crombach et al., 2012b), gene circuits were visually inspected for defects in gene expression profiles (Figure S4). See Table S3 for an overview of the number of gene circuits that passed each test for the different scenarios considered. The resulting sets of successful fits that were used for further analysis—20 solutions for the '0.065' scenario in *M. abdita*, and 20 solutions for *D. melanogaster*—are shown in Figure S5.

We have previously documented the most commonly observed defects for *D. melanogaster* circuits (Crombach et al., 2012b). Here, we categorise the defects for models fit to data from *M. abdita*. Although defects in either species show some similarities, they are not easily comparable or interpretable in a biologically meaningful way. Therefore, we refrain from a detailed analysis and only describe how particular defects were used to select circuits for further analysis. These are the most commonly observed problems in *M. abdita* circuits:

- Displaced expression boundaries (Panel A in Figure S4): the central feature of the gap gene system is to precisely regulate the location of gap gene expression domains. Hence, the misalignment of

domain boundaries in model output compared to expression data is generally regarded as a severe flaw.

- Ectopic expression domains (Panel B in Figure S4): occasionally, gap genes are expressed in regions where we know from experiments that there is no such expression. In general, this is considered a severe problem, though we discuss a specific exception below.

- Bimodal expression domains (Panel C in Figure S4): if gene expression domains show a persistent two- (or multi-)peaked profile, we discard the gene circuit.

- Mismatch of gene expression levels (Panel D in Figure S4): although it is considered a less severe flaw than displaced boundaries, mismatch of gene expression levels can be drastic enough to warrant the exclusion of a gene circuit from further analysis. In the most extreme case, the affected expression domain is entirely missing.

We find that each of the *M. abdita* gap genes exhibits stereotypical flaws in a subset of gene circuits. Some of these problems occur in virtually all circuits (Figure S5). We discuss these defects sorted by gap gene domain, in anterior to posterior order.

- The anterior domain of *gt* is usually reproduced correctly, with an accurately placed posterior boundary. However, in virtually all gene circuits this domain tends to have low expression levels during late time classes of C14A, and anterior *gt* expression disappears prematurely (Figure S5).

- In a subset of circuits, the anterior *hb* expression domain shifts abruptly in the anterior direction during C12–C13, after which its boundary remains constant. These circuits were not considered for analysis (not shown).

- The central *Kr* domain is generally positioned correctly. However, subsets of circuits exhibit excessively high early expression levels, and/or low expression at later time points, close to the onset of gastrulation (T8) (Figure S5). Depending on the severity of the expression level mismatch, we include or exclude these circuits for further analysis.

- We find a slight temporary displacement of the abdominal *kni* domain in most circuits. For early time points (before C14A), we observe an anteriorly displaced posterior border and/or posteriorly displaced anterior border, resulting in a slightly narrowed early domain of expression (not shown). We discarded circuits in which this defect was deemed severe. Yet, some displacement of early *kni* boundaries appears to be present in all circuits.

- The most commonly observed defect of the posterior *gt* domain is a mismatch of expression levels between models and data (Figure S5). All gene circuits show relatively low *gt* expression throughout the entire blastoderm stage. In a subset of circuits, we also observe a posterior displacement of the anterior domain boundary. The degree of severity of this defect differs quite smoothly between circuits (Figure S5).

- The posterior *hb* domain may show a transient bimodal pattern early on, while at later stages, some circuits show a slight posterior displacement of the domain. All circuits show a somewhat premature retraction of *hb* expression from the posterior pole region (Figure S5).

In addition, some circuits show a slight late ectopic expression of *Kr* and/or *kni* in the posterior terminal region (Panel B in Figure S4, and Figure S5). This defect is also frequently observed in *D. melanogaster* circuits (Crombach et al., 2012b). It is caused by a lack of *tll* expression, which in turn is due to the fact that we use mRNA expression data instead of the more extensive protein domain of *tll*. We select circuits showing this defect only if regulatory analysis finds that the ectopic domain does not substantially influence the expression dynamics in the terminal region.

Computational tools

A set of Python scripts (http://www.python.org) were used for data (post-)processing, preparing configuration files for the reverse-engineering procedure, and subsequent gene circuit analysis and visualisation. All code is available upon request.

Regulatory analysis of *M. abdita* gap gene circuits

In this section, we provide additional analysis of *M. abdita* gene circuits. We characterise the regulatory mechanisms that dynamically position gap domain boundaries in the trunk region of the *M. abdita* blastoderm embryo. We compare these mechanisms to *D. melanogaster*, and provide references to the relevant literature. Our analysis is based on examining the distribution of estimated parameter values, which characterise overall regulatory structure and strength of individual interactions, as well as a detailed graphical analysis of regulatory contributions to particular domain boundaries at specific points in space and time. Detailed discussions of *D. melanogaster* gene circuits in light of genetic and molecular experimental evidence have been published previously (Ashyraliyev et al., 2009; Crombach et al., 2012b; Jaeger et al., 2004a,b).

We structure our regulatory analysis in two alternative ways: the first one is guided by the fact that the gap gene system of *D. melanogaster* implements five distinct regulatory mechanisms (see Fig. 1 in the main paper) (Jaeger, 2011): (i) activation of gap genes by maternal gradients, (ii) gap gene auto-activation, (iii) strong mutual repression between gap genes with complementary expression domains (*hb*/*kni* and *Kr*/*gt*; alternating cushions), (iv) weaker repression with posterior bias among gap genes with overlapping domains (shift mechanism), and (v) repression of gap genes by terminal gap genes. While auto-activation varies strongly between solutions (except for *hb*; see also below), all circuits show the alternating cushions mechanism of strong mutual repression, and most circuits (except for the two extreme Bcd scale scenarios) implement domain shift mechanisms in a consistent manner in both species (Table S4). Only regulatory weights for the effect of terminal gap genes *tll* and *hkb* are extremely variable across solutions and scenarios (mechanism (v); not shown). This is due to the extensive overlap between expression patterns of these two genes in *M. abdita* (Wotton et al., 2015b), which leads to indeterminacy during model fitting. For this reason, we refrain from interpreting these interactions in terms of their biological significance and focus on the other regulatory mechanisms instead. The consistency and robustness of our results regarding mechanisms (i–iv) is further corroborated by analysis of parameter distributions (Figure S6 and Figure S7).

Taken together, the consistent implementation of essential regulatory mechanisms, and a clear trend towards predicted consensus network interactions, indicates that the overall qualitative structure of the gap gene network is strongly conserved between species. Only a small number of interactions differ in their regulatory sign in *M. abdita* compared to *D. melanogaster* circuits. Therefore, we focus on quantitative differences in regulatory strengths and expression dynamics between species. In what follows, we mainly use the '0.065' scenario for *M. abdita* (see Sections and for discussion). We provide a description of the regulatory mechanisms underlying the dynamic positioning of the anterior *gt* domain boundary; we elaborate on the qualitatively different regulatory mechanisms of the *hb-Kr* interface and *gt-hb* interface; and we address the posterior boundary of the posterior *hb* domain.

The Anterior *gt* Domain

The anterior domain of *gt* is special, in that its posterior boundary shifts very little (*D. melanogaster*) or not at all (*M. abdita*) (Wotton et al., 2015b). It is regulated in a very similar manner in both species. In *M. abdita* gene circuits, we observe activation of *gt* by Bcd (with a negligibly small additional contribution by Cad), combined with *gt* self-activation. In *D. melanogaster*, *gt* is activated predominantly by Bcd as well. However, self-regulation is not supported in this species: depending on the gene circuit, we observe slight activation, a lack of auto-regulation, or even inhibition. Activation by Bcd is supported by experiments knocking down *bcd* by RNA interference (RNAi) in *M. abdita*. These experiments show a marked reduction of anterior *gt* expression (Wotton et al., 2015c). Similarly, anterior *gt* is absent in *D. melanogaster* embryos derived from *bcd* mutant mothers (Eldon and Pirrotta, 1991; Kraut and Levine, 1991b; Tautz, 1988). There is no evidence on *gt* auto-activation in *M. abdita*. In *D. melanogaster*, a slight delay in the intensification of the late *gt* pattern (Eldon and Pirrotta, 1991), and the fact that Gt protein binds *gt* regulatory regions (Schroeder et al., 2004) may indicate the presence of weak or moderate auto-activation.

In *M. abdita* as in *D. melanogaster* gene circuits, both Hb and Kr inhibit *gt* expression, and limit the extent of the anterior *gt* domain (not shown). Repression by Kr is more pronounced in both species. It is part of an 'alternating cushions' mechanisms consisting of mutually repressive positive feedback loops between non-overlapping gap gene domains (Jaeger, 2011; Kraut and Levine, 1991b). This is entirely consistent with evidence from RNAi knock-down experiments, which show a strong posterior expansion of anterior *gt* in the case of *Kr*, and a much weaker one in the case of *hb* knock-down (Wotton et al., 2015b). In *D. melanogaster*, expansion of *gt* in *Kr* mutants was reported in some studies (Capovilla et al., 1992; Eldon and Pirrotta, 1991; Kraut and Levine, 1991b; Mohler et al., 1989), while a recent quantitative analysis did not detect this effect (Surkova et al., 2013). Repression of *gt* by Hb is supported by a slight expansion of anterior *gt* in *hb* mutants (Eldon and Pirrotta, 1991; Kraut and Levine, 1991b), and the complete absence of *gt* expression in embryo over-expressing *hb* (Kraut and Levine, 1991a).

Two modelling artifacts in the anterior region of the embryo are worth mentioning here: First, in our *M. abdita* models, anterior expression of *gt* diminishes over time in late C14A (from T6 onward), and by T8, it has nearly disappeared (Figure S5). Although this trend can also been seen in expression data (Wotton et al., 2015a,b), it is, in its severity, probably an artifact of the model. Second, many *D. melanogaster* models fit to mRNA data show a repressive effect of *gt* on anterior *hb* expression, causing a dip in *hb* expression levels (Crombach et al., 2012b). This is likely to be a modelling artifact, due to the complex regulation of *hb* from two independent promoters (Driever and Nüsslein-Volhard, 1988a,b; Margolis et al., 1994, 1995; Schröder et al., 1988; Struhl, 1989), which is not represented in our models. We never observe this effect in *M. abdita* gene circuits (Figure S5).

The *hb-Kr* Interface

This interface consists of the overlapping posterior boundary of anterior *hb* and the anterior boundary of the central *Kr* domain. It is of special interest due to the dynamic positioning of the posterior *hb* boundary in *M. abdita*, while this boundary remains static in *D. melanogaster* (Fig. 2C–E in the main paper). An analysis of these inter-species differences is presented in the main text (see Fig. 3A–D). Here, we provide a more detailed discussion.

Activation of both *hb* and *Kr* by Bcd is conserved in gene circuits for both species. For *M. abdita*, activation of *hb* by Bcd has been confirmed by RNAi knock-down and transgenic reporter assays, testing the expression of *M. abdita* regulatory elements in *D. melanogaster* (Lemke et al., 2008; Stauber et al., 2000; Wotton et al., 2015c). Furthermore, *Kr* is absent in strong knock-down phenotypes treated with *bcd* RNAi (Wotton et al., 2015c). In *D. melanogaster*, the anterior *hb* domain is absent—though a duplicated posterior *hb* domain is present in the anterior—in embryos derived from *bcd* mutant mothers (Driever and Nüsslein-Volhard, 1988a,b; Schröder et al., 1988; Tautz, 1988), and although the situation is a bit more complicated for *Kr*, there is good evidence that Bcd binds and activates its regulatory elements (Hoch et al., 1990, 1991; Hülskamp et al., 1990; Kraut and Levine, 1991a).

Activating inputs being conserved, we can explain the altered dynamics of *hb* expression between the two species through a combination of changed repressive regulatory interactions and differences in the initial placement of gap domain boundaries. In *M. abdita*, *hb* mRNA extends to 50% A–P position at the start of C12, while it only covers the anterior region of the embryo up to 45% during C13 in *D. melanogaster* (Figure S5). Subsequently, the *hb* boundary shifts anteriorly in *M. abdita*, from 50% A–P position at C12 to 42% at C14A-T8 (see Fig. 2C–E in the main text Wotton et al., 2015b). In contrast, this boundary remains stationary at 45% in *D. melanogaster*, gradually sharpening over time due to the repressive influence of *Kr* (Crombach et al., 2012b; Houchmandzadeh et al., 2002; Jaeger et al., 2004a,b; Surkova et al., 2008).

Our models provide a mechanistic explanation for this difference in expression dynamics (see Fig. 3A–D in the main paper and Figure S8, Figure S9). Repressive interactions between *hb* and *Kr* are weaker in *M. abdita* than in *D. melanogaster* (see Fig. 2F in the main text). This enables a wide initial overlap between the two domains and explains why *hb* can extend so far to the posterior, far into the central *Kr* domain. Weak repression by Kr in the resulting zone of overlap gradually lowers the expression level of *hb* by subtly changing the balance between repression and activation. Lower levels of Hb allow *kni*

to become activated, overcoming its initial inhibition by *hb*. Very strong repression of *hb* by Kni then causes the complete down-regulation of *hb*, resulting in the observed shift of the boundary in *M. abdita*. This mechanism is strongly supported by experimental evidence from *M. abdita* showing that the *hb* boundary is displaced posteriorly in both *Kr* and *kni* RNAi knock-down embryos (Wotton et al., 2015b).

In contrast, much stronger repressive feedback between *hb* and *Kr* prevents any substantial overlap between domains at any time during the blastoderm stage in *D. melanogaster* (Clyde et al., 2003; Gaul et al., 1987; Hülskamp et al., 1990; Jäckle et al., 1986). This double-negative (positive) feedback locks nuclei into either expressing *hb* or *Kr*, thus maintaining a stable *hb* boundary in this species (Jaeger et al., 2004b). In addition, the relative difference in repression strength by Kr and Kni is much less pronounced in this species, and while either of these factors is essential to control boundary position in *M. abdita*, their regulatory roles are much more redundant in *D. melanogaster*. This is consistent with the observation that neither single mutants of *Kr* nor *kni* exhibit any unambiguous posterior displacement of the *hb* boundary (Houchmandzadeh et al., 2002; Jäckle et al., 1986). Only eliminating both factors at the same time leads to a clearly detectable de-repression of *hb* in *D. melanogaster* (Clyde et al., 2003; Manu et al., 2009b; Surkova et al., 2013).

In summary, the difference between the two species depends on altered overlaps between the domains and the relative strength of *hb* repression by Kr. In *M. abdita*, this interaction is weak, which counter-intuitively leads to a shifting boundary. In contrast, it is much stronger in *D. melanogaster*, especially when considered in relation to repression by Kni, which leads to much more redundancy between *Kr* and *kni* and a stationary *hb* boundary in this species.

The Posterior *gt-hb* Interface

This interface is discussed in the main text (Fig. 3E–H,J and Figure S14, Figure S15). We observe that the posterior boundary of the posterior *gt* domain shows very different shift dynamics in the two species (Fig. 2C–E in the main text). While it progresses at a constant rate throughout C14A in *D. melanogaster*, its retraction from the pole is delayed until T3/4 in *M. abdita*. This delay is later compensated by an accelerated shift rate compared to *D. melanogaster*. In both species, the anterior shift of the posterior *gt* domain is caused by up-regulation of posterior *hb* expression (Eldon and Pirrotta, 1991; Kraut and Levine, 1991b; Mohler et al., 1989; Wotton et al., 2015b) (Figure S14, Figure S15).

Consistent with this, *hb* transcripts accumulate at a quite constant rate in the posterior region of *D. melanogaster* embryos, while *hb* expression is suddenly initiated around T2/3 in *M. abdita* (Wotton et al., 2015b) (Fig. 3G,H of the main paper). This difference in *hb* expression dynamics depends predominantly on the mechanism of its activation. *M. abdita* gene circuits exhibit two phases of *hb* activation in the posterior of the embryo: initially, weak auto-activation is boosted in the zone of overlap between *hb* and *gt* through additional activation by Gt. At later stages, *hb* auto-activation comes to dominate. The two phases can clearly be distinguished in Fig. 3G of the main paper (see also Figure S14). In contrast to the 'pull-and-trigger' two-phase mechanism, *D. melanogaster* models show strong *hb* auto-activation throughout C14A: Gt represses *hb*, no substantial overlap exists between *gt* and *hb* domains, and no separate phases of regulation are evident (Fig. 3H of the main paper, Figure S15). This difference is supported by experimental evidence: the posterior *hb* domain is reduced in *gt* RNAi knock-down embryos of *M. abdita* (Wotton et al., 2015b), while posterior *hb* is not affected in *D. melanogaster* *gt* mutants (Eldon and Pirrotta, 1991; Strunk et al., 2001).

Interestingly, *D. melanogaster* gene circuits fit to protein expression data show activation of *hb* by Gt in contrast to our current models fitted to mRNA (Ashyraliyev et al., 2009; Jaeger et al., 2004a,b). However, in *D. melanogaster* protein circuits *hb* auto-activation is strong, and we cannot detect any two-phase regulation of *gt* as in *M. abdita*. This suggests that the difference between the dynamics of *M. abdita* and *D. melanogaster* circuits can be mainly explained by the amount of overlap of the *gt* and *hb* expression domain, in combination with the altered strength of *hb* auto-activation.

The Posterior Boundary of the Posterior *hb* Domain

In *D. melanogaster*, Hkb repression regulates the posterior boundary of the posterior *hb* domain and its retraction from the embryonic pole (Brönner and Jäckle, 1991; Casanova, 1990). RNAi knock-down experiments indicate that the role of the terminal gap genes is more redundant in *M. abdita*: although Hkb is also required for the retraction of the posterior *hb* domain in this species, Tll provides additional repressive contributions (Wotton et al., 2015b).

This redundancy is reflected in the much more extensive overlap between *hkb* and *tll* mRNA domains in *M. abdita* compared to *D. melanogaster* (Wotton et al., 2015b). Such similarity may explain the pronounced lack of parameter determinability affecting the regulatory weights for Hkb and Tll in *M. abdita* models (Figure S2, compare scenario '0.065' with others). Lack of determinability, in turn, leads to frequent defects and variability in the placement of the posterior boundary of posterior *hb* (see Figure S5 and discussion in Section). For these reasons, we cannot analyse the regulatory behaviour of this boundary with our current models. It is possible—but far from certain, given the extensive regulatory redundancy reported in (Wotton et al., 2015b)—that protein expression data for the two terminal gap genes may alleviate this problem in the future.

Robustness of modelling results to parameter perturbations

We discuss a number of numerical experiments we performed to test the robustness of our results against variations in model parameters. In particular, we compare gene circuits based on Bcd gradients with different scales (see Section), models with no diffusion or self-regulation of gap genes, and the effect of not fixing threshold parameters h^a to specific values (see Section). The number of optimisation runs performed and the number of solutions selected for further analysis in each scenario are summarised in Table S3.

Varying Bcd Gradient Scale

We first tested the sensitivity of our results with regard to differing scales for the Bcd gradient. As described in Section , exponential approximations to the Bcd gradient are characterised by their slope or decay parameter λ. For *M. abdita*, we generated five differently scaled gradients, centred around the measured slope of the Bcd gradient in *D. melanogaster*: $\lambda_{Ma} \in \{0.050, 0.060, 0.065, 0.070, 0.080\}$. Smaller values of λ generate a shallower gradient, i.e. a gradient that reaches further posteriorly, while larger values create a steeper gradient along the A–P axis. Our regulatory analysis in Section mainly uses $\lambda_{Ma} = 0.065$. Here we focus on the other scenarios.

All scenarios produce good fitting solutions (Table S3) with extremely similar gene expression dynamics (data not shown). In particular, both the shifting posterior boundary of *hb*, and the altered dynamics of the posterior *gt-hb* interface are reproduced correctly by all circuits. This is reflected by the underlying parameter values. All circuits in all scenarios reproduce the mutual repression mechanism (alternating cushions) and we see only slight variations in the presence or absence of specific boundary shift mechanisms between scenarios (Table S4). Furthermore, the genetic interconnectivity matrices shown in Figure S2 are extremely similar across Bcd gradient scenarios. Values for λ_{Ma} of 0.060, 0.065, and 0.070 all yield exactly the same predicted consensus regulatory network structure. The two extreme scenarios with λ_{Ma} of 0.050 and 0.080 show slight structural variations, such as absence of *kni* auto-activation and activation of *hb* by Cad for 0.050, or absence of weak repression of *gt* by Kni and repression of *Kr* by Hb for 0.080. None of these interactions are essential for correct gap gene expression (see Section for a more detailed discussion).

Finally, *D. melanogaster* gene circuits presented in this paper differ slightly from those published previously in Crombach et al. (2012b) in that we use a time-dependent approximation of the Bcd gradient in this study (see Section). Again, predicted consensus regulatory network structure is extremely similar between the two sets of models. The only interactions that vary are *gt* auto-activation (absent in our current circuits; not relevant for correct gap gene expression), and activation of *kni* by Bcd, which

had been reproduced incorrectly in our earlier models, probably due to the use of a less realistic time-invariant Bcd gradient approximation.

In summary, our results establish that both network structure and gene expression profiles derived from *M. abdita* and *D. melanogaster* gap gene circuit models are robust towards variations in Bcd gradient approximations.

Gap Gene Circuits Without Diffusion

Previous studies have shown that patterning in *D. melanogaster* gap gene circuits fit to protein data does not depend on diffusion of gap gene products (Jaeger et al., 2004b; Manu et al., 2009a). These circuits still produce a correct spatio-temporal arrangement of gap domains when diffusion is switched off, although domain shapes are more rugged than in simulations with diffusion. In contrast, gap gene circuits fit to mRNA data from *D. melanogaster* and *M. abdita* show a series of severe patterning defects if diffusion is set to zero (not shown). For instance, such circuits often exhibit split *Kr* and/or *kni* domains.

For this reason, we used an alternative approach to test whether patterning relies on diffusion in mRNA-based circuits. We performed a series of optimisation runs for *M. abdita*, during which all diffusion parameters D^a were fixed to zero. This leads to a drastic decrease in the number of successful fitting solutions and resulting circuits generally have higher RMS scores than those with diffusion (Table S3). Despite all this, several circuits still fit the data correctly. These circuits show accurate positioning and timing of gap domains, although expression patterns are less smooth than in circuits with diffusion (not shown). Furthermore, diffusion-less circuits predict the same regulatory mechanisms and network structure as models with diffusion. The only exceptions affect gap gene auto-regulation and activation of *hb* by Gt, which is also variable across Bcd gradient scenarios (see above). None of these interactions are essential for correct gap gene expression (see Section , for detailed discussion). Equivalent results were obtained by fitting *D. melanogaster* circuits without diffusion (not shown).

In summary, our results indicate that diffusion is not essential for position and timing of gap boundaries. This corroborates earlier analyses (Jaeger et al., 2004b; Manu et al., 2009a) showing that gap gene patterning in *D. melanogaster* is not a diffusion- but a reaction-driven process.

Gap Gene Circuits Without Auto-Regulation

We have previously shown that patterning in the *D. melanogaster* blastoderm does not depend on gap gene auto-regulation, since gene circuits with all auto-regulatory terms set to zero correctly reproduce timing and placement of gap domains (Perkins et al., 2006). This largely also applies to models for *M. abdita*. To our surprise, we even found that fixing self-regulatory parameters to zero during optimisation increases the fraction of successful fits (Table S3): out of 100 runs, we obtained 26 gene circuits for further analysis, compared to about 5 in 100 for other scenarios.

However, there are subtle differences between the two species that are worth pointing out. In contrast to models in *D. melanogaster*, *M. abdita* gene circuits without auto-regulation do show several slight patterning defects (not shown). First, the posterior boundary of the posterior *hb* domain fails to retract from the pole in many fitting solutions. This defect is not specific to auto-regulation, however, since the same problem occurs in gene circuits with diffusion (Figure S5). Second, the posterior *gt* domain is slightly displaced towards the posterior. This is due to a failure of the 'pull-and-trigger' mechanism for boundary shifts in the *gt-hb* interface (see Fig. 3E–H of the main paper, and Section). This mechanism relies on late-stage *hb* auto-activation for its two-phase dynamical behaviour. In addition, *gt* expression levels are often low in comparison with other gap genes, due to repression by *hb* in its anterior domain. The latter two defects are specific to gene circuits without auto-regulation.

A comparison of interconnectivity matrices between circuits with and without auto-regulation confirms that both models implement largely the same regulatory mechanisms (not shown). Only two interactions differ: (i) there is no repression of *Kr* by Hb, which is inconsequential since it is entirely

consistent with the shift mechanism for the posterior *hb* boundary discussed in the main text (Fig. 3A–D) and Section above; (ii) Gt does not activate *hb*, which is due to the absence of the 'pull-and-trigger' mechanism for the retraction of posterior *gt* in circuits without auto-regulation. While causing patterning defects in the posterior, lack of this interaction prevents excessive activation of *hb* (and hence repression of *gt*) in the anterior region of the embryo.

In summary, our results largely corroborate the analysis of *D. melanogaster* gene circuits in Perkins et al. (2006), demonstrating that auto-regulation does not play any major role in gap gene patterning in *M. abdita*. However, unlike *D. melanogaster*, auto-regulation *is* required in *M. abdita* circuits for the correct shift of the *gt-hb* interface in the posterior region of the embryo.

Fixing Threshold Parameters, h^a

Earlier studies in *D. melanogaster* have shown that threshold parameters h^a (see Methods of main text) are difficult to determine by model fitting, since ubiquitous activation encoded by positive h^a parameter values are redundant with activating contributions from maternal gradients (Ashyraliyev et al., 2009; Jaeger et al., 2004a,b). For this reason, we usually fix h^a parameters to saturating negative values (in our circuits: $h^a = -2.5$) during optimisation.

We adopt the same strategy for fitting *M. abdita* circuits. h^a were set to -2.5 during optimisation. We validated this choice by performing a small series of fits in which we allow h^a parameter values to be optimised. This does not improve optimisation performance: only very few gene circuits finish with an acceptable RMS score, which is generally higher than in runs with fixed h^a parameter values. This suggests that correlations between h^a and other parameters negatively affect the fitting algorithm, as observed for *D. melanogaster* circuits. All resulting fitting solutions exhibited expression defects that would exclude them from further analysis. Finally, all circuits with acceptable RMS scores show h^a values that are negative. In summary, we conclude that fixing h^a to -2.5 is a reasonable modelling choice.

Supplementary Figures and Tables

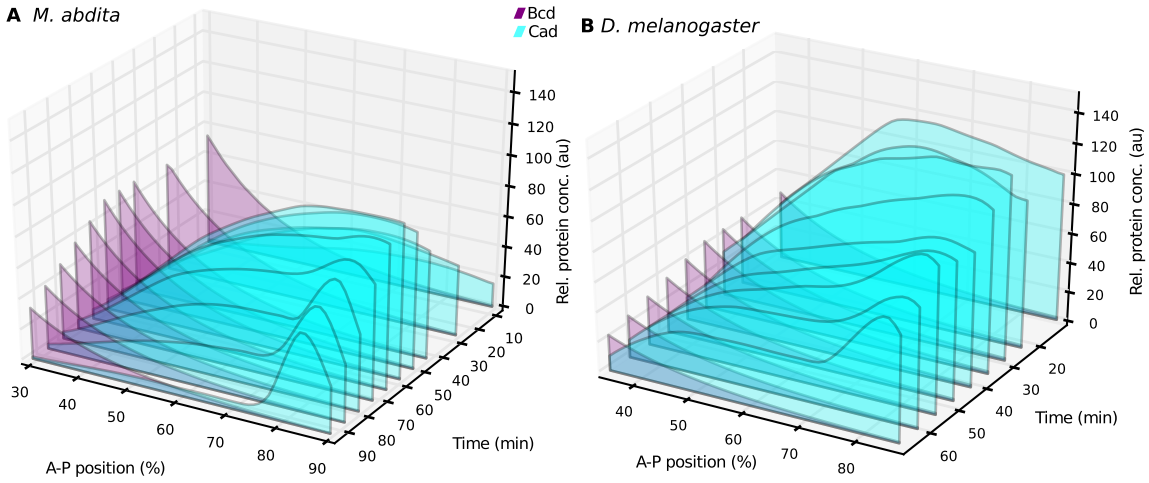

Supplementary Figure 1. Estimated protein expression patterns of maternal co-ordinate genes *bcd* (purple) and *cad* (cyan). Space-time plots of expression profiles are shown for *M. abdita* (A) and *D. melanogaster* (B). X-axes represent % A–P position, where 0% is the anterior pole. Y-axes represent time in minutes (min). Z-axes represent relative protein concentration in arbitrary units (au). See S1 Text for details on how protein profiles were estimated/approximated.

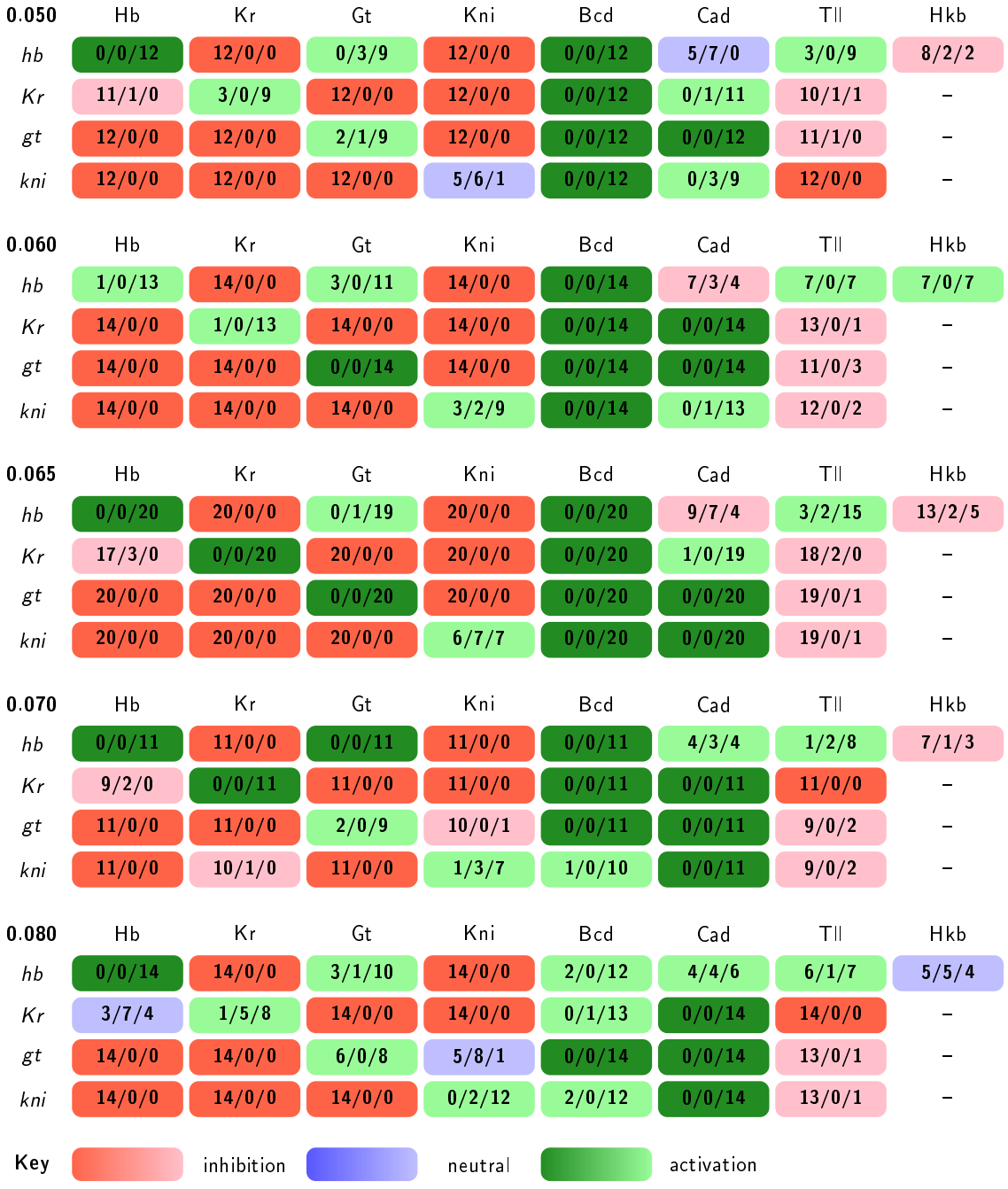

Supplementary Figure 2. Genetic interconnectivity matrices for scenarios with different *M. abdita* Bcd gradients. Regulatory parameters from independently fit gene circuits were categorised by their values. Columns represent regulators; rows target genes. An interaction is considered repressive if it value is < -0.005, activating if > 0.005, and neutral (no interaction) otherwise. Number triplets indicate the number of gene circuits with repressive/neutral/activating interactions. Background colours indicate if a majority of parameters were repressive (red), activating (green), or neutral (blue); dark colours indicate cases where all gene circuits show identical behaviour, light colours indicate cases where parameters fall into distinct categories in different circuits.

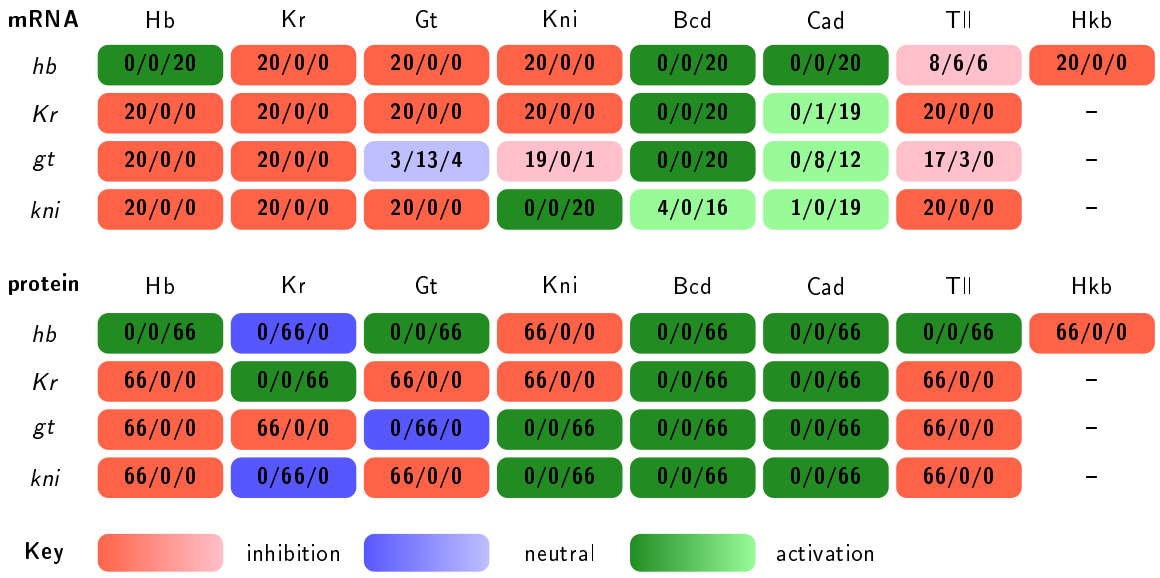

Supplementary Figure 3. Genetic interconnectivity matrices for *D. melanogaster* gene circuits fit to mRNA or protein data. Representation of matrices as in Figure S2 The interconnectivity matrix for protein-based circuits has been published previously in Ashyraliyev et al. (2009) and is shown for comparison.

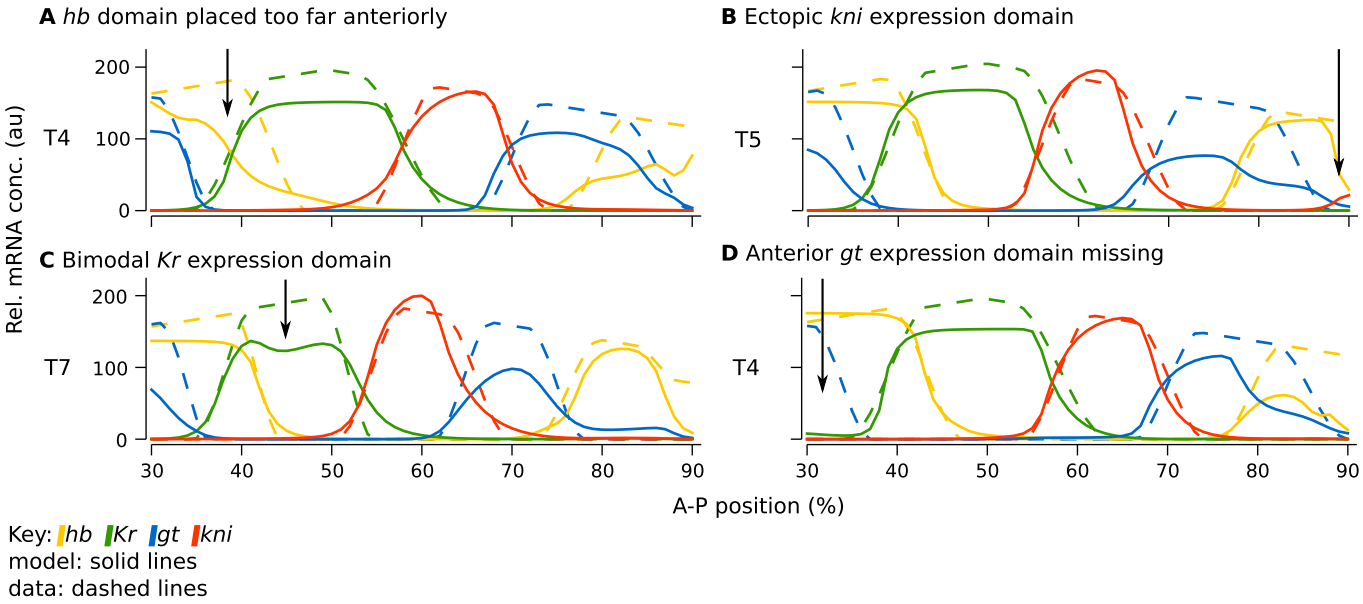

Supplementary Figure 4. Common gene expression defects in *M. abdita* gene circuits. Plots show model output (solid lines) and expression data (dashed lines). (A) some gene circuits exhibit defects in boundary placement and/or dynamics. Here, we show an example where the posterior boundary of the anterior *hb* domain is misshapen and displaced towards the anterior (arrow). We rejected such circuits. (B) some gene circuits show small ectopic expression domains. Here *kni* is miss-expressed in the posterior pole region (arrow). We discarded such circuits only if analysis of the model revealed that the ectopic domain significantly affects gene regulation. (C) some gene circuits show domains with multiple peaks of expression. Our example shows a bimodal central *Kr* domain (arrow). We excluded such circuits from further analysis. (D) some gene circuits show severe defects in expression levels. We show an extreme example where the anterior *gt* domain is completely missing (arrow). Such circuits were only discarded if miss-expression is severe. Horizontal axes represent % A–P position (where 0% is the anterior pole). Vertical axes show relative mRNA concentrations in arbitrary units (au). T4/5/7 represent time classes during C14A.

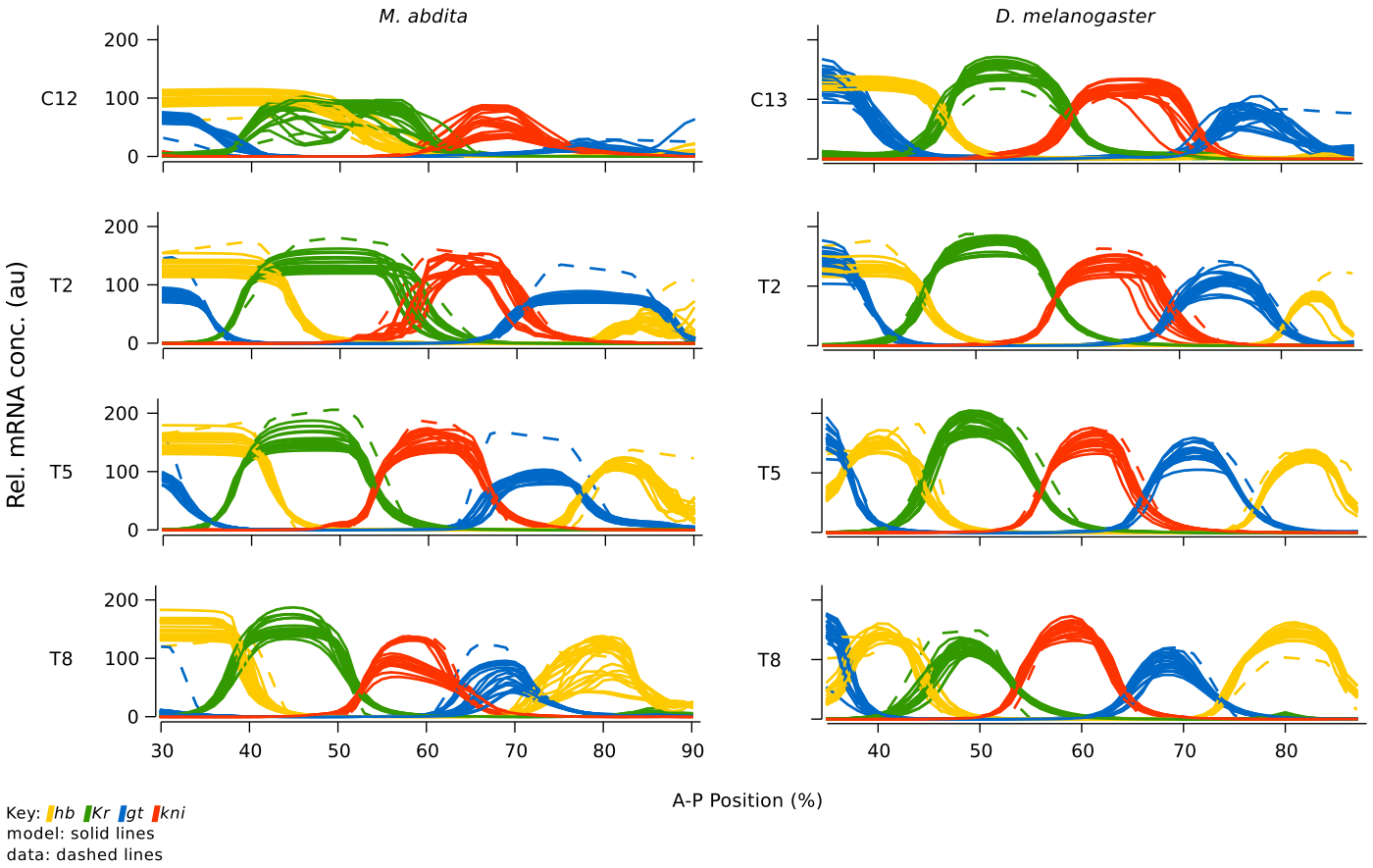

Supplementary Figure 5. Gene circuit fits to data in *M. abdita* and *D. melanogaster* (see also Fig. 2C–E, in the main paper). Plots show model output (solid lines) displayed against expression data (dashed lines). For both species, we show all 20 fits selected for final analysis (see Table S3). Horizontal axes represent % A–P position (where 0% is the anterior pole). Vertical axes show relative mRNA concentration in arbitrary units (au). *M. abdita* circuits cover cycles C12–C14A, *D. melanogaster* circuits C13 and C14A due to earlier onset of gap gene expression in the former. C12 (C13) represents mitotic cycle 12 (13), T2/5/8 represent time classes during C14A; time progresses downwards in both columns.

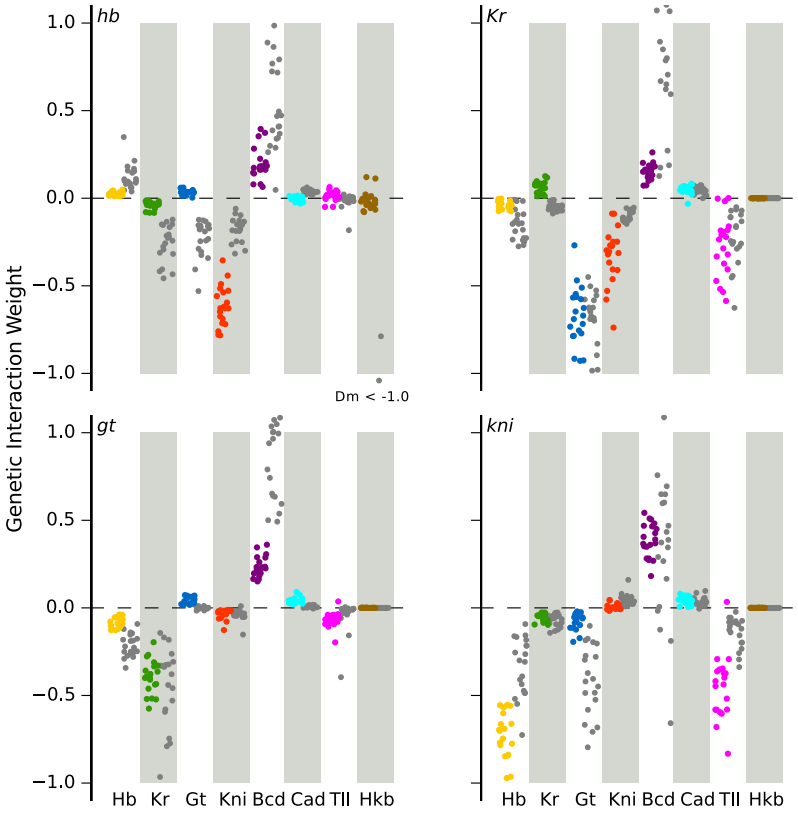

Supplementary Figure 6. Comparison of interaction strengths for all regulatory weights across species. Scatter plots show distribution of estimated parameter values from fitted and selected circuits (see Table S3). For *M. abdita*, we show scenario $\lambda_{Ma} = 0.065$ (coloured dots). *D. melanogaster* distributions are shown in grey for comparison. Target genes are separated by panel with columns representing regulators (indicated along the X-axes). Note that most repressive weights for Hkb on *hb* fall outside the displayed area, since this interaction is strongly negative (values < -1.0).

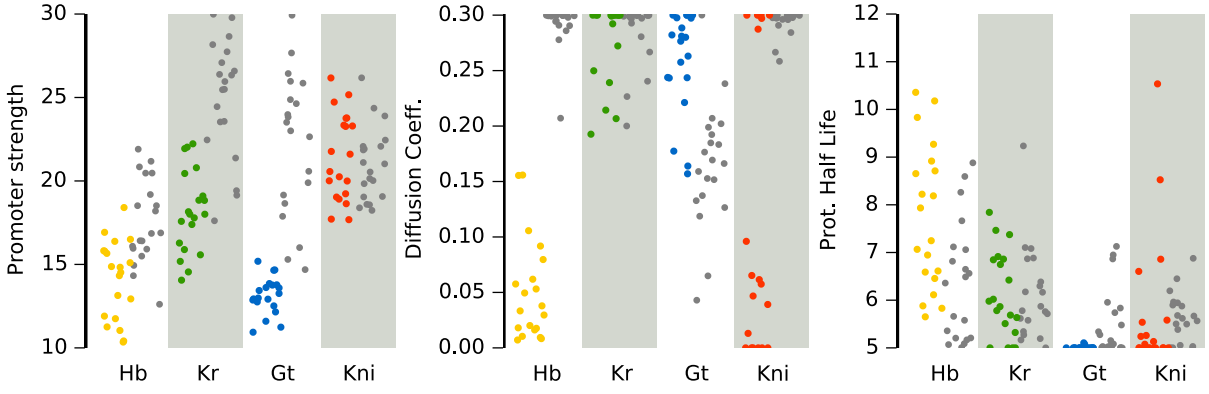

Supplementary Figure 7. Comparison of maximum production rates, diffusion parameters, and gene product half lives between species. Scatter plots show distribution of estimated parameter values from fitted and selected circuits (see Table S3). For *M. abdita*, we show scenario $\lambda_{Ma} = 0.065$ (coloured dots). *D. melanogaster* distributions are shown in grey for comparison. Panels are arranged by parameter; genes are indicated along the X-axes. Maximum production rates are limited to the range $[10.0,\ 30.0]$, diffusion coefficients to the range $[0.0,\ 0.3]$, and half lives to the range $[5.0,\ 20.0]$.

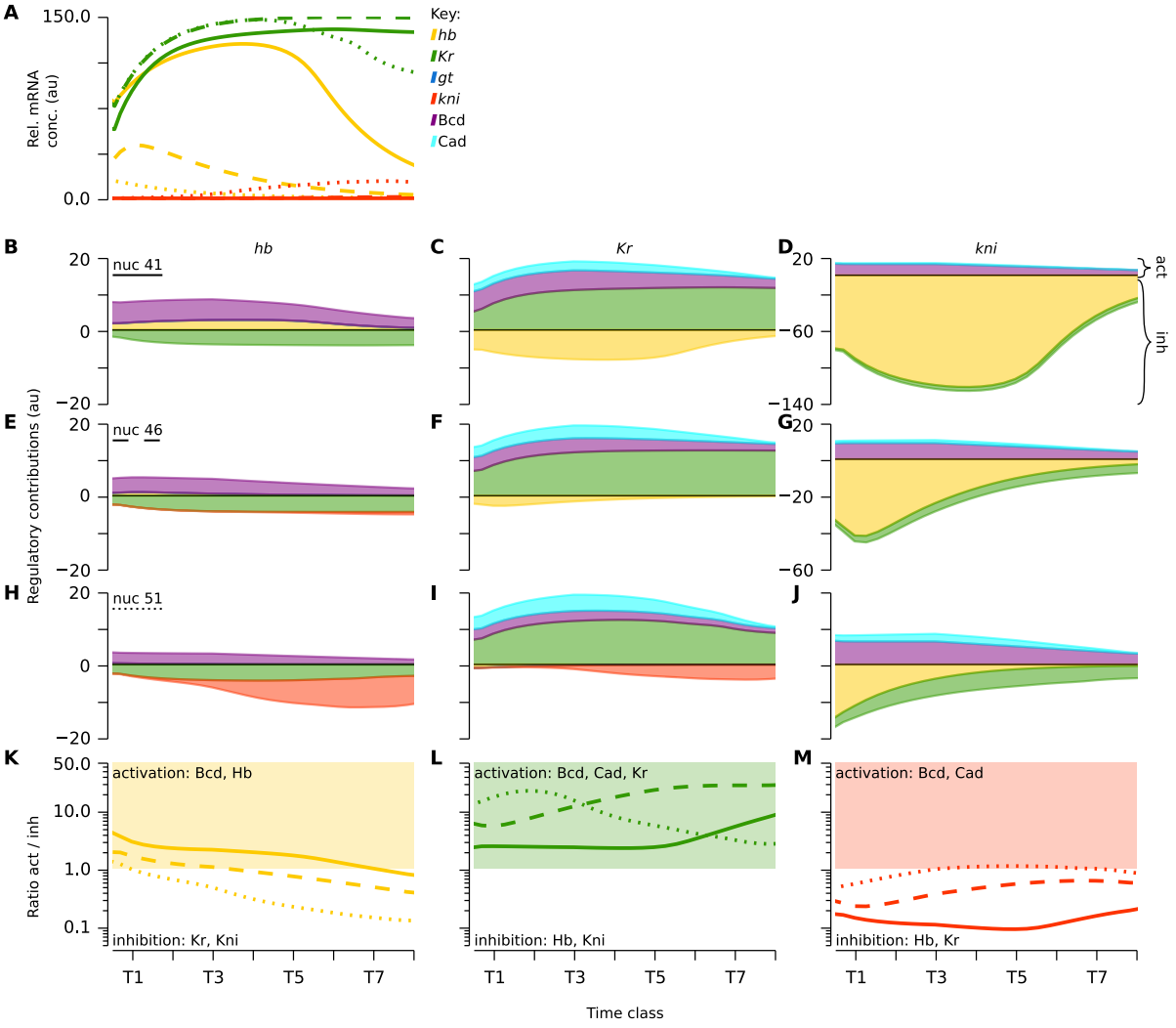

Supplementary Figure 8. Graphical analysis of the *hb-Kr* interface in *M. abdita*. (A) gene expression levels over time of *hb* (yellow), *Kr* (green), and *kni* (red) in nuclei within the shift zone at 41% (solid), 46% (dashed), and 51% (dotted) A–P position. The shift of the posterior *hb* boundary is visible as a posterior-to-anterior succession in the onset of *hb* repression. (B to J) time plots showing accumulative regulatory contributions of gap genes and external inputs to *hb* (B, E, H), *Kr* (C, F, I), and *kni* (D, G, J) (see Materials and methods for equations and precise definitions). Activating contributions are >0.0 and inhibiting contributions are <0.0 (see D). (K to M) the ratio of activating to repressing contributions over time in nuclei as given in (A). Light yellow, green or red areas indicate net activation; white areas net repression. See main text for a description of the ratchet-like shift mechanism. In all graphs, horizontal axes represent time, covering mitotic cycle C14A (T1–T8). Vertical axes represent relative mRNA concentrations or regulatory contributions in arbitrary units (au), except for (K to M) where vertical axes represent log-scale ratios of activation versus repression.

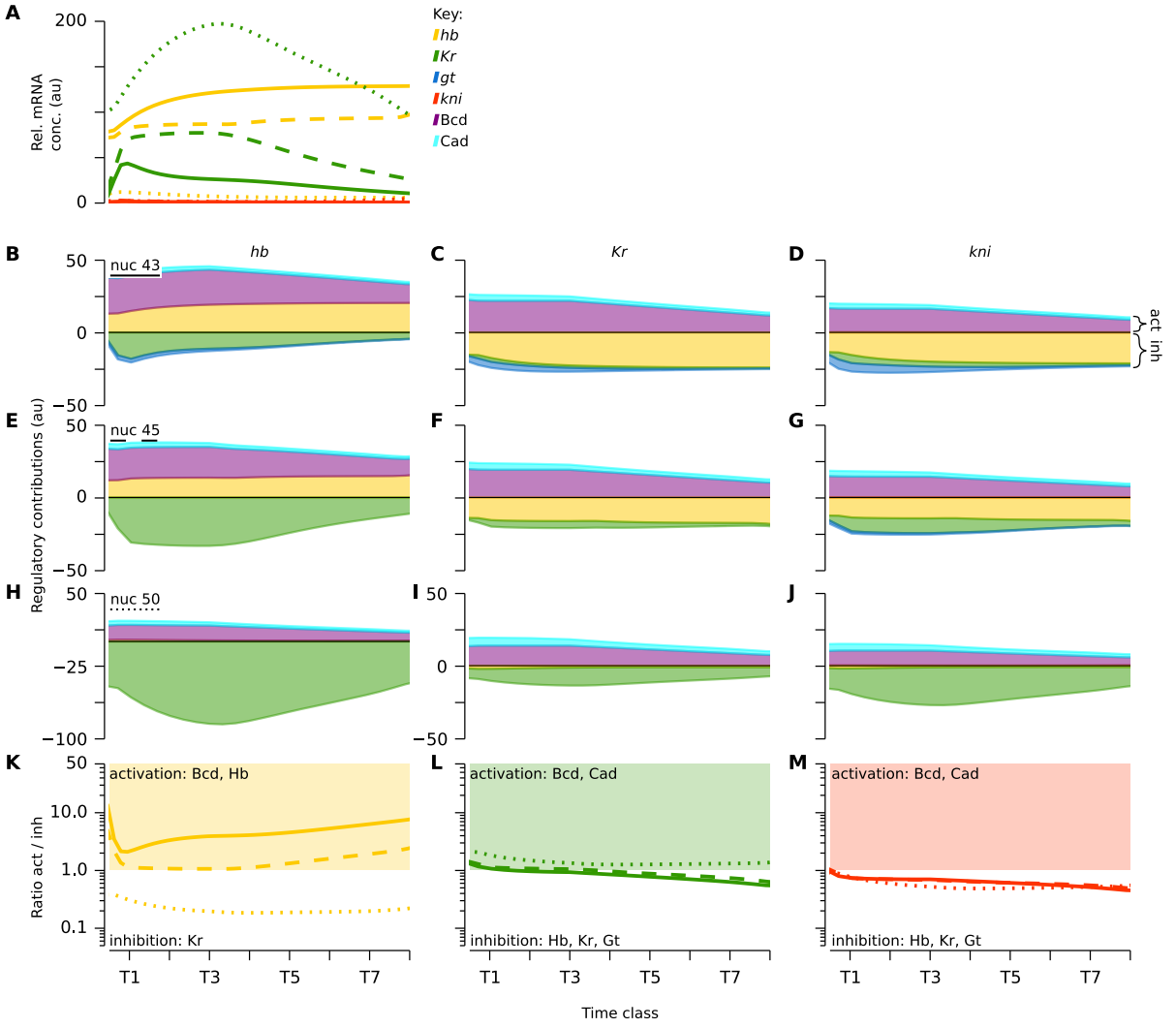

Supplementary Figure 9. Graphical analysis of the *hb-Kr* interface in *D. melanogaster*. (A) gene expression levels over time of *hb* (yellow), *Kr* (green), and *kni* (red) in nuclei within the boundary interface at 43% (solid), 45% (dashed), and 50% (dotted) A–P position. Stable expression levels of *hb* indicate a stationary *hb* boundary. (B to J) time plots showing accumulative regulatory contributions of gap genes and external inputs to *hb* (B, E, H), *Kr* (C, F, I), and *kni* (D, G, J) (see Materials and methods for equations and precise definitions). Activating contributions are >0.0 and inhibiting contributions are <0.0 (see D). In contrast to *M. abdita* (Figure S8), the posterior boundary of anterior *hb* remains stationary in *D. melanogaster* due to strong regulatory feedback between *hb* and *Kr*. *kni* is not actively involved in positioning this boundary in wild-type, but can supplant *Kr* repression in *Kr* mutants (not shown). (K to M) the ratio of activating to repressing contributions over time in nuclei as given in (A). Light yellow, green or red areas indicate net activation; white areas net repression. In contrast to *M. abdita* (Figure S8), nuclei maintain a stable activation-to-repression balance over time. In all graphs, horizontal axes represent time, covering mitotic cycle C14A (T1–T8). Vertical axes represent relative mRNA concentrations or regulatory contributions in arbitrary units (au), except for (K to M) where vertical axes represent log-scale ratios of activation versus repression.

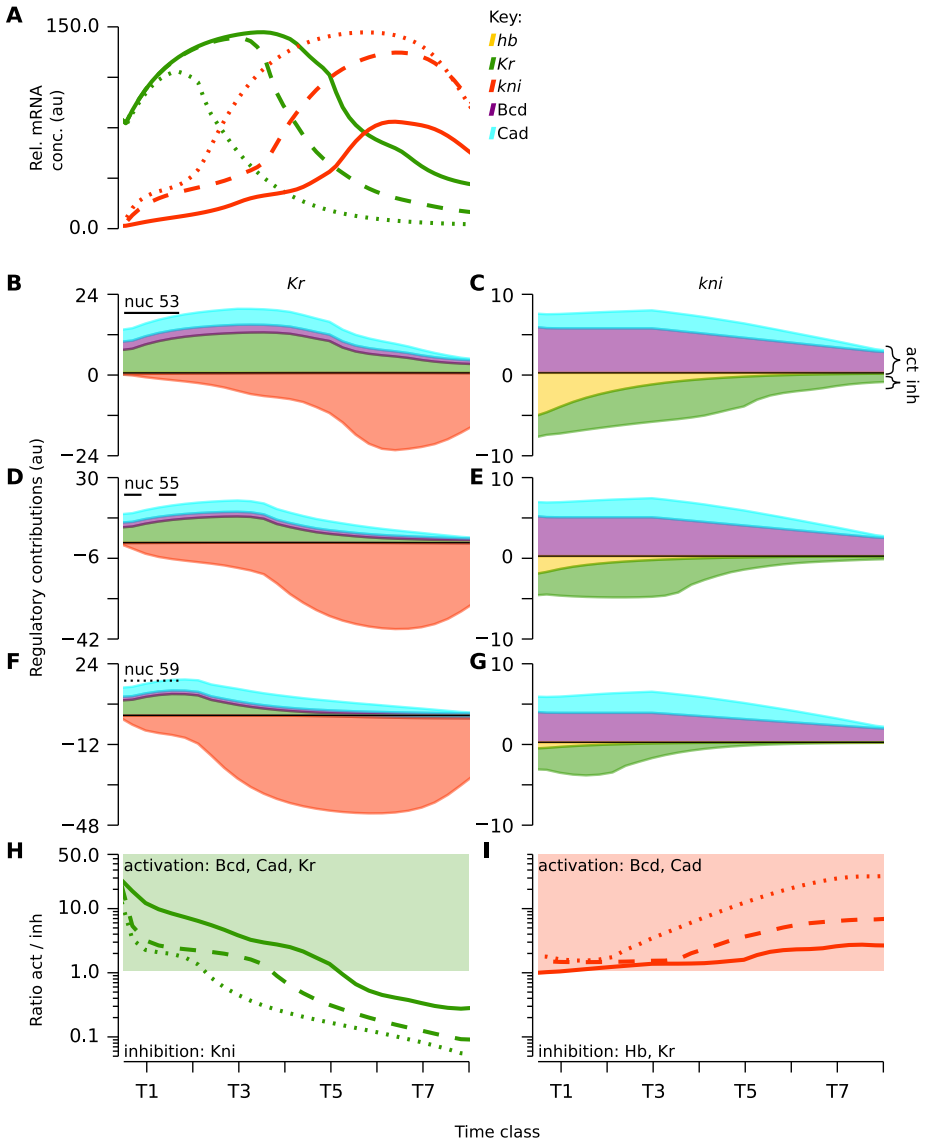

Supplementary Figure 10. Graphical analysis of the *Kr-kni* interface in *M. abdita*. (A) gene expression levels over time of *Kr* (green) and *kni* (red) in nuclei within the shift zone at 53% (solid), 55% (dashed), and 59% (dotted) A–P position. Boundary shifts are visible as a posterior-to-anterior succession of *Kr* down- and *kni* up-regulation. (B to G) time plots showing accumulative regulatory contributions of gap genes and external inputs to *Kr* (B, D, F) and *kni* (C, E, G) (see Materials and methods for equations and precise definitions). Activating contributions are >0.0 and inhibiting contributions are <0.0 (see E). Boundary shifts occur due to the asymmetry between strong repression of *Kr* by Kni (B, D, F) versus weaker repression of *kni* by Kr (C, E, G). (H, I) the ratio of activating to repressing contributions over time in nuclei as given in (A). Light green or red areas indicate net activation; white areas net repression. In all graphs, horizontal axes represent time, covering mitotic cycle C14A (T1–T8). Vertical axes represent relative mRNA concentrations or regulatory contributions in arbitrary units (au), except for (H, I) where vertical axes represent log-scale ratios of activation versus repression.

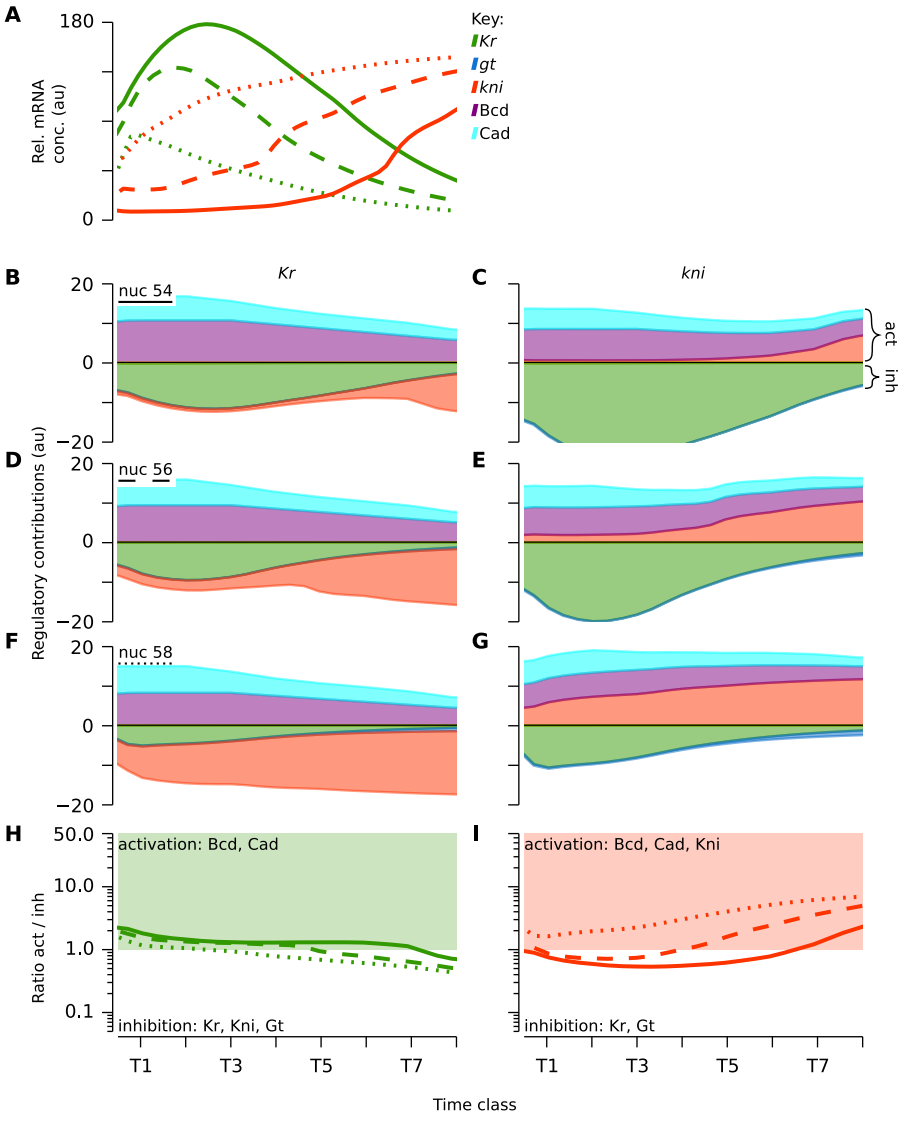

Supplementary Figure 11. Graphical analysis of the *Kr-kni* interface in *D. melanogaster*. (A) gene expression levels over time of *Kr* (green) and *kni* (red) in nuclei within the shift zone at 54% (solid), 56% (dashed), and 58% (dotted) A–P position. Boundary shifts are visible as a posterior-to-anterior succession of *Kr* down- and *kni* up-regulation, similar to *M. abdita* (Figure S10). (B to G) time plots showing accumulative regulatory contributions of gap genes and external inputs to *Kr* (B, D, F) and *kni* (C, E, G) (see Materials and methods for equations and precise definitions). Activating contributions are >0.0 and inhibiting contributions are <0.0 (see C). The asymmetry between repression of *Kr* by Kni (B, D, F) and repression of *kni* by Kr (C, E, G) is less pronounced than in *M. abdita* (S10), yet–in combination with *Kr* auto-repression and *kni* auto-activation–still sufficient to tip the regulatory balance between the two genes. This can be seen in (H, I) which show the ratio of activating to repressing contributions over time in nuclei as given in (A). Light green or red areas indicate net activation; white areas net repression. Despite subtle differences in shift mechanism and dynamics, the overall behaviour of the switch between *Kr* and *kni* is similar to *M. abdita* (S10). In all graphs, horizontal axes represent time, covering mitotic cycle C14A (T1–T8). Vertical axes represent relative mRNA concentrations or regulatory contributions in arbitrary units (au), except for (H, I) where vertical axes represent log-scale ratios of activation versus repression.

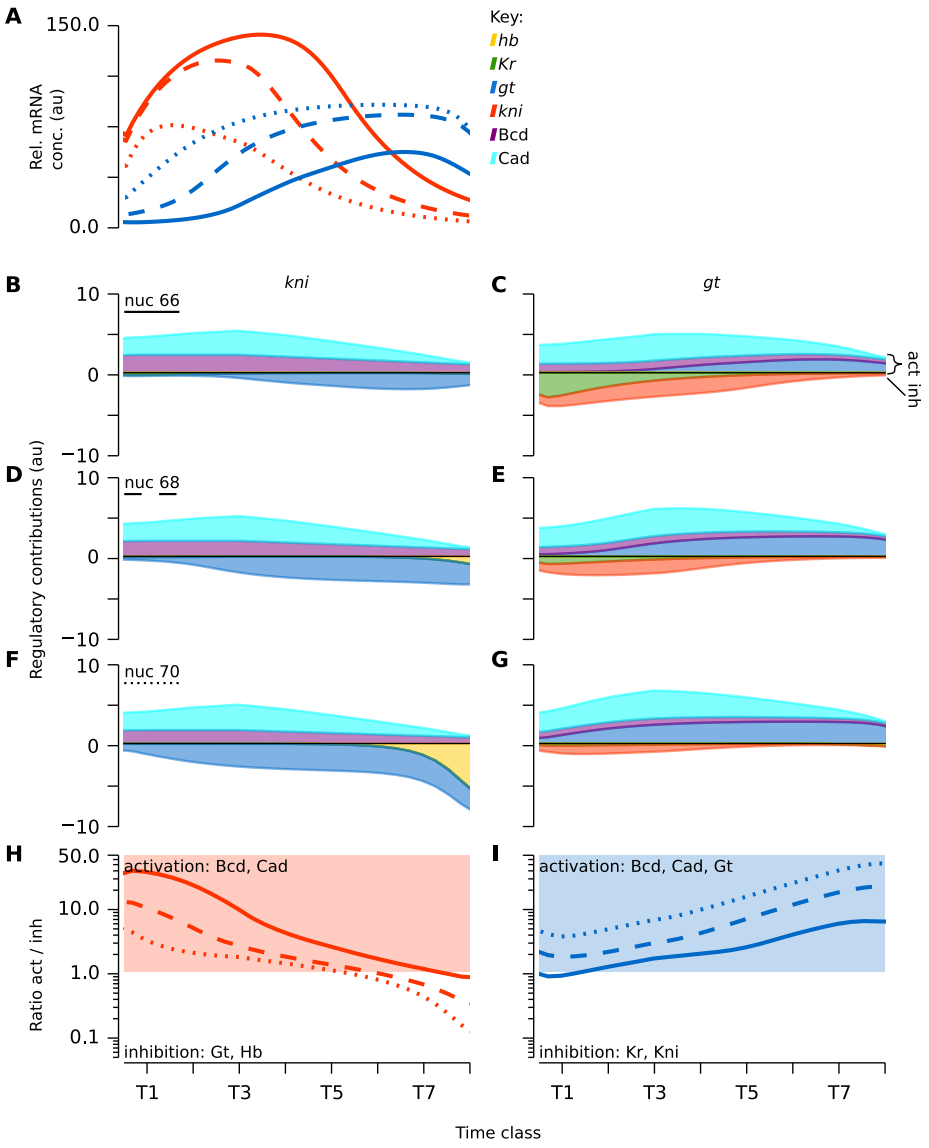

Supplementary Figure 12. Graphical analysis of the *kni-gt* interface in *M. abdita*. (A) gene expression levels over time of *kni* (red) and *gt* (blue) in nuclei within the shift zone at 66% (solid), 68% (dashed), and 70% (dotted) A–P position. Boundary shifts are visible as a posterior-to-anterior succession of *kni* down- and *gt* up-regulation. (B to G) time plots showing accumulative regulatory contributions of gap genes and external inputs to *kni* (B, D, F) and *gt* (C, E, G) (see Materials and methods for equations and precise definitions). Activating contributions are >0.0 and inhibiting contributions are <0.0 (see C). Boundary shifts occur due to the asymmetry between repression of *kni* by Gt (B, D, F) versus repression of *gt* by Kni (C, E, G). In 11 out of 20 circuits, Hb further represses *kni* in posterior nuclei at late stages (G). (H, I) the ratio of activating to repressing contributions over time in nuclei as given in (A). Light red or blue coloured areas indicate net activation; white areas net repression. In all graphs, horizontal axes represent time, covering mitotic cycle C14A (T1–T8). Vertical axes represent relative mRNA concentrations or regulatory contributions in arbitrary units (au), except for (H, I) where vertical axes represent log-scale ratios of activation versus repression.

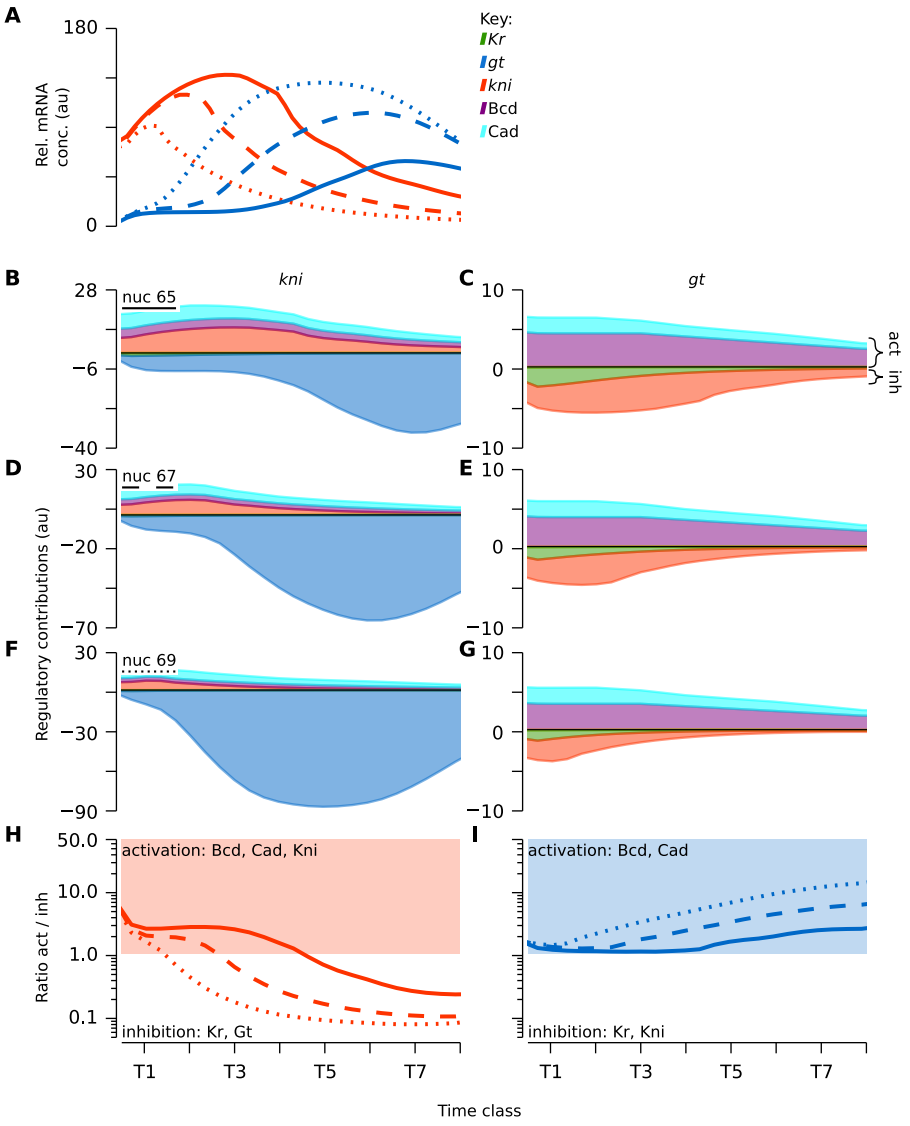

Supplementary Figure 13. Graphical analysis of the *kni-gt* interface in *D. melanogaster*. (A) gene expression levels over time of *kni* (red) and *gt* (blue) in nuclei within the shift zone at 65% (solid), 67% (dashed), and 69% (dotted) A–P position. Boundary shifts are visible as a posterior-to-anterior succession of *Kr* down- and *kni* up-regulation, similar to *M. abdita* (Figure S12). (B to G) time plots showing accumulative regulatory contributions of gap genes and external inputs to *kni* (B, D, F) and *gt* (C, E, G) (see Materials and methods for equations and precise definitions). Activating contributions are >0.0 and inhibiting contributions are <0.0 (see C). Boundary shifts are caused by strong asymmetry between repression of *kni* by Gt (B, D, F) and repression of *gt* by Kni (C, E, G). In *D. melanogaster*, we never observe an additional late repressive contribution by Hb, as seen in half of *M. abdita* circuits (Figure S12. (H, I) the ratio of activating to repressing contributions over time in nuclei as given in (A). Light red or blue coloured areas indicate net activation; white areas net repression. Despite subtle differences in mechanism and dynamics, the overall behaviour of the switch between *kni* and *gt* is similar to *M. abdita* (Figure S12). In all graphs, horizontal axes represent time, covering mitotic cycle C14A (T1–T8). Vertical axes represent relative mRNA concentrations or regulatory contributions in arbitrary units (au), except for (H, I) where vertical axes represent log-scale ratios of activation versus repression.

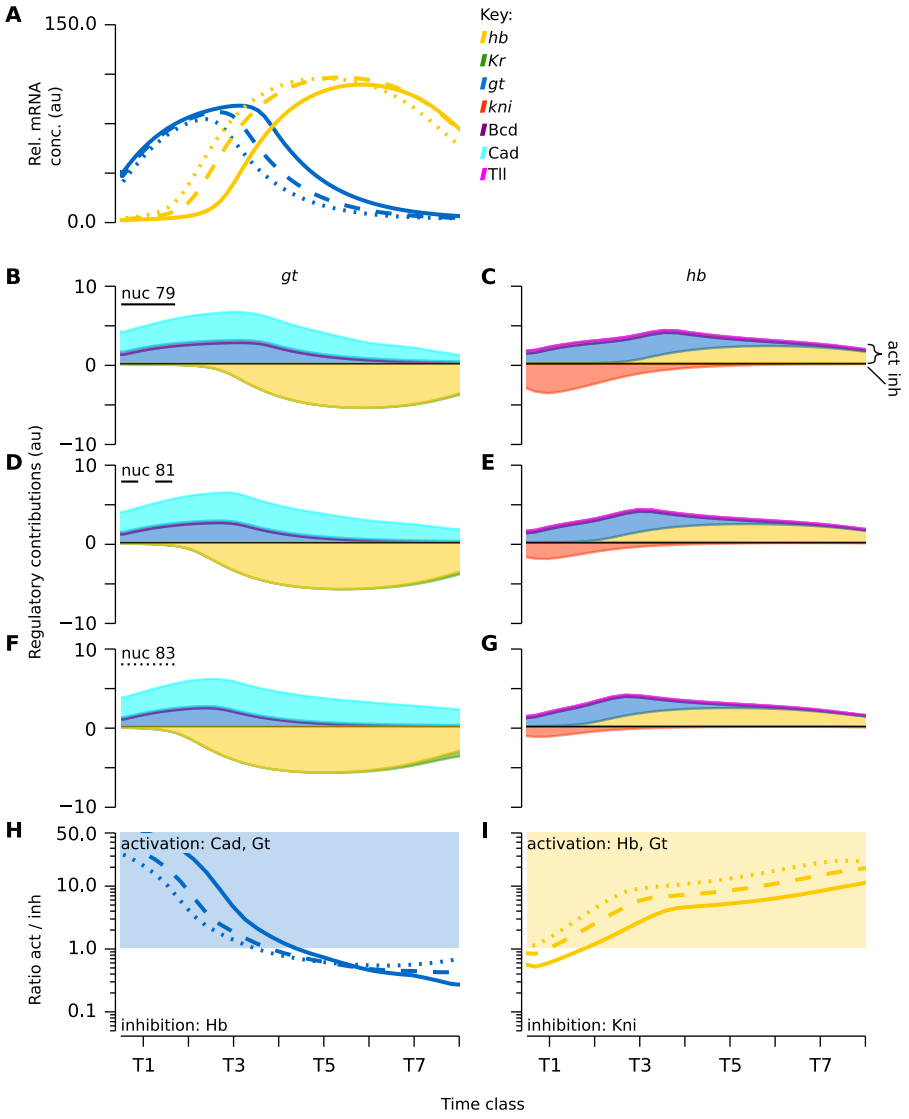

Supplementary Figure 14. Graphical analysis of the *gt-hb* interface in *M. abdita*. (A) gene expression levels over time of *gt* (blue) and *hb* (yellow) in nuclei within the shift zone at 79% (solid), 81% (dashed), and 83% (dotted) A–P position. Two-phase dynamics of boundary shifts are clearly visible as sudden *gt* down- and concomitant *hb* up-regulation at mid cycle C14A. (B to G) time plots showing accumulative regulatory contributions of gap genes and external inputs to *gt* (B, D, F) and *hb* (C, E, G) (see Materials and methods for equations and precise definitions). Activating contributions are >0.0 and inhibiting contributions are <0.0 (see C). Early activation by Gt is later replaced by *hb* auto-activation (B, D, F). (H, I) the ratio of activating to repressing contributions over time in nuclei as given in (A). Light blue or yellow coloured areas indicate net activation; white areas net repression. Two distinct phases of *hb* regulation are clearly visible in (I); they coincide with the switch from Gt activation to *hb* auto-activation in (C, E, G). See main text for further description of this 'pull-and-trigger' two-phase shift mechanism. In all graphs, horizontal axes represent time, covering mitotic cycle C14A (T1–T8). Vertical axes represent relative mRNA concentrations or regulatory contributions in arbitrary units (au), except for (H, I) where vertical axes represent log-scale ratios of activation versus repression.

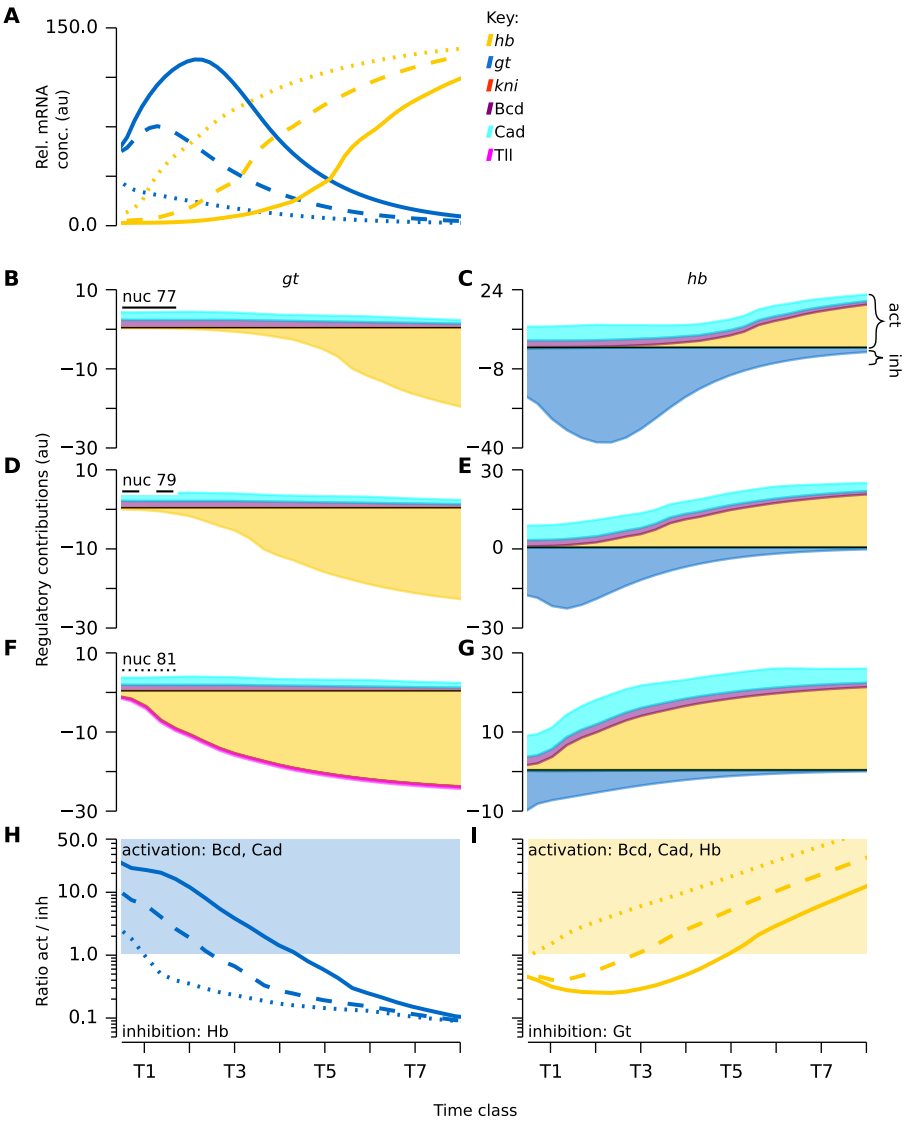

Supplementary Figure 15. Graphical analysis of the *gt-hb* interface in *D. melanogaster*. (A) gene expression levels over time of *gt* (blue) and *hb* (yellow) in nuclei within the shift zone at 77% (solid), 79% (dashed), and 81% (dotted) A–P position. The switch from *gt* to *hb* expression occurs much more gradually and at different times in different nuclei in *D. melanogaster* compared to *M. abdita* (Figure S14). (B to G) time plots showing accumulative regulatory contributions of gap genes and external inputs to *gt* (B, D, F) and hb (C, E, G) (see Materials and methods for equations and precise definitions). Activating contributions are >0.0 and inhibiting contributions are <0.0 (see C). Strong *hb* auto-activation is visible at early stages in posterior nuclei (E, G). This is not the case in *M. abdita* circuits, where auto-activation suddenly increases around T3 or T4 (Figure S14). (H, I) the ratio of activating to repressing contributions over time in nuclei as given in (A). Light blue or yellow coloured areas indicate net activation; white areas net repression. In contrast to *M. abdita* (Figure S14), the switch from activation to repression (and vice versa) happens much more gradually. In all graphs, horizontal axes represent time, covering mitotic cycle C14A (T1–T8). Vertical axes represent relative mRNA concentrations or regulatory contributions in arbitrary units (au), except for (H, I) where vertical axes represent log-scale ratios of activation versus repression.

Species	Embryos	Boundary	
		Start	End
M. abdita	20	2.555	33.043
D. melanogaster	85	4.493	20.476

Supplementary Table 1. Extent of the *bcd* mRNA domain. The first column indicates the species. The second column shows the number of embryos for which we measured the extent of localised *bcd* mRNA using the data processing pipeline described in (Crombach et al., 2012a). Average start and end positions for the *bcd* domain are shown in columns three and four, respectively. Numbers represent % A–P position, where 0% is the anterior pole of the embryo.

Mitotic Cycle	Time Class	*M. abdita* time	*D. melanogaster* time	Description
		0.000		division C11
C12		8.000		interphase
		11.500		mitosis
		16.000	0.000	division
C13		28.750	10.550	interphase
		37.000	16.500	mitosis
		41.500	21.100	division
C14A	T1	45.073	24.225	interphase
	T2	52.219	30.475	
	T3	59.365	36.725	
	T4	66.511	42.975	
	T5	73.656	49.225	
	T6	80.802	55.475	
	T7	87.948	61.725	
	T8	95.094	67.975	
		98.667	71.100	gastrulation

Supplementary Table 2. Mitotic division schedules and time classes for *M. abdita* and *D. melanogaster*. For *M. abdita*, we use the timing of developmental events derived from a single high quality time-lapse video in which the transitions between the different phases of the cell cycle were clearly visible. This represents an individual developmental trajectory, consistent with our staging scheme for *M. abdita* (Wotton et al., 2014). For *D. melanogaster*, the schedule was taken from Crombach et al. (2012b) which is itself based on earlier modelling work (Ashyraliyev et al., 2009; Jaeger et al., 2004a,b) and a detailed characterisation of embryogenesis using live imaging microscopy (Foe, 1989; Foe and Alberts, 1983). Mitoses are incorporated into gene circuits as three different regimes (see also Methods): during 'interphase' continuous dynamics are governed by equations which contain terms for regulated production, diffusion, and degradation of gene products; during 'mitosis' the regulatory term is set to zero and there is only diffusion and degradation. Finally, 'division' is an instantaneous event at which the number of nuclei, and hence the number of equations in the system, is doubled. Time in minutes, C12–C14A: cleavage cycles 12 to 14A; T1–8 indicate time classes used for model fitting during C14A.

Species	Scenario	Runs	Numerically OK	RMS < 30.0	Analysis
M. abdita	0.050	200	171	36	12
	0.060	200	170	44	14
	0.065	400	320	89	20
	0.070	200	168	55	11
	0.080	200	161	54	14
	no diffusion	300	286	44*	7
	no auto-regulation	100	87	38	26
	h parameter	50	39	4	0
D. melanogaster		225	169	140	20

Supplementary Table 3. Selection of gene circuits for analysis. The first column indicates the name of the species. The second column indicates the fitting scenario. The first five scenarios are named according to the value of the decay parameter for the *M. abdita* Bcd gradient λ_{Ma} (see S1 Text); "no diffusion" are gene circuits fit with fixed diffusion parameters $D^a = 0$; "no auto-regulation" are gene circuits fit to data with all auto-regulatory weights in W set to zero; "*h* parameter" are *M. abdita* circuits with threshold parameters not fixed to a specific value (S1 Text)(Crombach et al., 2012b). For each scenario, we report the total number of gene circuit models fit to data (third column), the number of gene circuits that passed our tests for numerical instability (fourth column), and the number of circuits that have a Root Mean Square (RMS) < 30.0 (< 35.0 for the "no diffusion" scenario, indicated by an asterisk; fifth column). The remaining runs were subjected to visual inspection for defects in expression profiles (see S1 Text). The number of gene circuits per scenario that passed this final test are given in column six.

Species	Scenario	Runs	Activation		Auto-activation				Mutual inhibition	Domain shift			
			Bcd	Cad	*hb*	*Kr*	*gt*	*kni*		*hb-Kr*	*Kr-kni*	*kni-gt*	*gt-hb*
M. abdita	0.050	12	12	9	12	9	9	1	12	6	12	9	12
	0.060	14	14	13	13	13	14	9	14	11	14	13	13
	0.065	20	20	20	20	19	19	5	20	20	20	19	20
	0.070	11	11	11	11	11	9	7	11	10	11	10	11
	0.080	14	12	14	14	8	8	12	14	5	14	14	14
D. melanogaster		20	20	12	20	0	4	20	20	9	20	20	15

Supplementary Table 4. Presence of patterning principles in *M. abdita* scenarios and *D. melanogaster* reference gene circuits. The first column indicates species. The second column lists fitting scenarios with different Bcd gradients as in Table S3. The third column indicates the total number of runs, or gene circuits, analysed for each scenario. Subsequent columns indicate how many of these circuits implement a specific regulatory principle as indicated on top. 'Activation' is defined as the number of gene circuits with Bcd activating *hb* and *Kr*, and with Cad activating *gt* and *kni*, respectively. 'Mutual inhibition' represents the presence of strong repression between *hb* and *kni*, as well as *Kr* and *gt*. The presence of a 'Domain shift' depends on net repressive balance between overlapping gap genes as described in (Crombach et al., 2012b).

References

Ashyraliyev, M., Siggens, K., Janssens, H., Blom, J., Akam, M., and Jaeger, J. (2009). Gene circuit analysis of the terminal gap gene *huckebein*. *PLoS Comput. Biol.*, 5(10):e1000548.

Brönner, G. and Jäckle, H. (1991). Control and function of terminal gap gene activity in the posterior pole region of the *Drosophila* embryo. *Mech. Dev.*, 35(3):205–211.

Capovilla, M., Eldon, E. D., and Pirrotta, V. (1992). The *giant* gene of *Drosophila* encodes a b-ZIP DNA-binding protein that regulates the expression of other segmentation gap genes. *Development*, 114(1):99–112.

Casanova, J. (1990). Pattern formation under the control of the terminal system in the *Drosophila* embryo. *Development*, 110(2):621–628.

Clyde, D. E., Corado, M. S. G., Wu, X., Paré, A., Papatsenko, D., and Small, S. (2003). A self-organizing system of repressor gradients establishes segmental complexity in *Drosophila*. *Nature*, 426:849–853.

Crombach, A., Cicin-Sain, D., Wotton, K. R., and Jaeger, J. (2012a). Medium-throughput processing of whole mount *in situ* hybridisation experiments into gene expression domains. *PLoS One*, 7(9):e46658.

Crombach, A., Wotton, K. R., Cicin-Sain, D., Ashyraliyev, M., and Jaeger, J. (2012b). Efficient reverse-engineering of a developmental gene regulatory network. *PLoS Comput. Biol.*, 8(7):e1002589.

Driever, W. and Nüsslein-Volhard, C. (1988a). The *bicoid* protein determines position in the *Drosophila* embryo in a concentration-dependent manner. *Cell*, 54:95–104.

Driever, W. and Nüsslein-Volhard, C. (1988b). A gradient of *bicoid* protein in *Drosophila* embryos. *Cell*, 54:83–93.

Eldon, E. D. and Pirrotta, V. (1991). Interactions of the *drosophila* gap gene *giant* with maternal and zygotic pattern-forming genes. *Development*, 111(2):367–378.

Foe, V. E. (1989). Mitotic domains reveal early commitment of cells in *Drosophila* embryos. *Development*, 107:1–22.

Foe, V. E. and Alberts, B. M. (1983). Studies of nuclear and cytoplasmic behaviour during the five mitotic cycles that precede gastrulation in *Drosophila* embryogenesis. *J. Cell Sci.*, 61:31–70.

Gaul, U., Seifert, E., Schuh, R., and Jäckle, H. (1987). Analysis of *Krüppel* protein distribution during early *Drosophila* development reveals posttranscriptional regulation. *Cell*, 50:639–647.

Gregor, T., Wieschaus, E. F., McGregor, A. P., Bialek, W., and Tank, D. W. (2007). Stability and nuclear dynamics of the *bicoid* morphogen gradient. *Cell*, 130:141–152.

Grimm, O., Coppey, M., and Wieschaus, E. (2010). Modelling the Bicoid gradient. *Development*, 137(14):2253–2264.

Hoch, M., Schröder, C., Seifert, E., and Jäckle, H. (1990). cis-acting control elements for *Krüppel* expression in the *Drosophila* embryo. *The EMBO Journal*, 9:2587–2595.

Hoch, M., Seifert, E., and Jäckle, H. (1991). Gene expression mediated by cis-acting sequences of the *Krüppel* gene in response to the *Drosophila* morphogens *bicoid* and *hunchback*. *The EMBO Journal*, 10:2267–2278.

Houchmandzadeh, B., Wieschaus, E., and Leibler, S. (2002). Establishment of developmental precision and proportions in the early *Drosophila* embryo. *Nature*, 415:798–802.

Hülskamp, M., Pfeifle, C., and Tautz, D. (1990). A morphogenetic gradient of *hunchback* protein organizes the expression of the gap genes *Krüppel* and *knirps* in the early *Drosophila* embryo. *Nature*, 346:577–580.

Jäckle, H., Tautz, D., Schuh, R., Seifert, E., and Lehmann, R. (1986). Cross-regulatory interactions among the gap genes of *Drosophila*. *Nature*, 324:668–670.

Jaeger, J. (2011). The gap gene network. *Cell. Mol. Life Sci.*, 68(2):243–274.

Jaeger, J., Blagov, M., Kosman, D., Kozlov, K. N., Manu, Myasnikova, E., Surkova, S., Vanario-Alonso, C. E., Samsonova, M., Sharp, D. H., and Reinitz, J. (2004a). Dynamical analysis of regulatory interactions in the gap gene system of *Drosophila melanogaster*. *Genetics*, 167(4):1721–1737.

Jaeger, J., Surkova, S., Blagov, M., Janssens, H., Kosman, D., Kozlov, K. N., Manu, Myasnikova, E., Vanario-Alonso, C. E., Samsonova, M., Sharp, D. H., and Reinitz, J. (2004b). Dynamic control of positional information in the early *Drosophila* embryo. *Nature*, 430(6997):368–371.

Kraut, R. and Levine, M. (1991a). Mutually repressive interactions between the gap genes *giant* and *Krüppel* define middle body regions of the *Drosophila* embryo. *Development*, 111:611–621.

Kraut, R. and Levine, M. (1991b). Spatial regulation of the gap gene *giant* during *Drosophila* development. *Development*, 111:601–609.

Lemke, S., Stauber, M., Shaw, P. J., Rafiqi, A. M., Prell, A., and Schmidt-Ott, U. (2008). *bicoid* occurrence and bicoid-dependent *hunchback* regulation in lower cyclorrhaphan flies. *Evol. Dev.*, 10:413–420.

Little, S. C., Tkačik, G., Kneeland, T. B., Wieschaus, E. F., and Gregor, T. (2011). The formation of the Bicoid morphogen gradient requires protein movement from anteriorly localized mRNA. *PLoS Biol.*, 9(3):e1000596.

Manu, Surkova, S., Spirov, A. V., Gursky, V. V., Janssens, H., Kim, A.-R., Radulescu, O., Vanario-Alonso, C. E., Sharp, D. H., Samsonova, M., and Reinitz, J. (2009a). Canalization of gene expression and domain shifts in the *Drosophila* blastoderm by dynamical attractors. *PLoS Comput. Biol.*, 5(3):e1000303.

Manu, Surkova, S., Spirov, A. V., Gursky, V. V., Janssens, H., Kim, A.-R., Radulescu, O., Vanario-Alonso, C. E., Sharp, D. H., Samsonova, M., and Reinitz, J. (2009b). Canalization of gene expression in the *Drosophila* blastoderm by gap gene cross regulation. *PLoS Biol.*, 7(3):e1000049.

Margolis, J. S., Borowsky, M. L., Shim, C. W., and Posakony, J. W. (1994). A small region surrounding the distal promoter of the *hunchback* gene directs maternal expression. *Dev. Biol.*, 163:381–388.

Margolis, J. S., Borowsky, M. L., Steingrimsson, E., Shim, C. W., Lengyel, J. A., and Posakony, J. W. (1995). Posterior stripe expression of *hunchback* is driven from two promoters by a common enhancer element. *Development*, 121:3067–3077.

Mlodzik, M. and Gehring, W. J. (1987). Expression of the *caudal* gene in the germ line of *Drosophila*: formation of an RNA and protein gradient during early embryogenesis. *Cell*, 48:465–478.

Mohler, J., Eldon, E. D., and Pirrotta, V. (1989). A novel spatial transcription pattern associated with the segmentation gene, *giant*, of *Drosophila*. *The EMBO Journal*, 8:1539–1548.

Moreno, E. and Morata, G. (1999). *caudal* is the hox gene that specifies the most posterior *Drosophila* segment. *Nature*, 400:873–877.

Perkins, T. J., Jaeger, J., Reinitz, J., and Glass, L. (2006). Reverse engineering the gap gene network of *Drosophila melanogaster*. *PLoS Comput. Biol.*, 2(5):e51.

Pisarev, A., Poustelnikova, E., Samsonova, M., and Reinitz, J. (2009). Flyex, the quantitative atlas on segmentation gene expression at cellular resolution. *Nucleic Acids Res.*, 37(Database issue):D560–D566.

Poustelnikova, E., Pisarev, A., Blagov, M., Samsonova, M., and Reinitz, J. (2004). A database for management of gene expression data in situ. *Bioinformatics*, 20:2212–2221.

Schröder, C., Tautz, D., Seifert, E., and Jäckle, H. (1988). Differential regulation of the two transcripts from the *Drosophila* gap segmentation gene *hunchback*. *The EMBO Journal*, 7:2881–2887.

Schroeder, M. D., Pearce, M., Fak, J., Fan, H. Q., Unnerstall, U., Emberly, E., Rajewsky, N., Siggia, E. D., and Gaul, U. (2004). Transcriptional control in the segmentation gene network of *Drosophila*. *PLoS Biol.*, 2:e271.

Schulz, C. and Tautz, D. (1995). Zygotic *caudal* regulation by *hunchback* and its role in abdominal segment formation of the *Drosophila* embryo. *Development*, 121:1023–1028.

Stauber, M., Jäckle, H., and Schmidt-Ott, U. (1999). The anterior determinant *bicoid* of *Drosophila* is a derived Hox class 3 gene. *Proc. Natl. Acad. Sci. U. S. A.*, 96(7):3786–3789.

Stauber, M., Lemke, S., and Schmidt-Ott, U. (2008). Expression and regulation of *caudal* in the lower cyclorrhaphan fly *Megaselia*. *Development, Genes and Evolution*, 218:81–87.

Stauber, M., Prell, A., and Schmidt-Ott, U. (2002). A single Hox3 gene with composite *bicoid* and *zerknüllt* expression characteristics in non-cyclorrhaphan flies. *Proc. Natl. Acad. Sci. U. S. A.*, 99:274–279.

Stauber, M., Taubert, H., and Schmidt-Ott, U. (2000). Function of *bicoid* and *hunchback* homologs in the basal cyclorrhaphan fly *Megaselia* (Phoridae). *Proc. Natl. Acad. Sci. U. S. A.*, 97(20):10844–10849.

Struhl, G. (1989). Differing strategies for organizing anterior and posterior body pattern in *Drosophila* embryos. *Nature*, 338:741–744.

Strunk, B., Struffi, P., Wright, K., Pabst, B., Thomas, J., Qin, L., and Arnosti, D. N. (2001). Role of ctBP in transcriptional repression by the *Drosophila giant* protein. *Dev. Biol.*, 239:229–240.

Surkova, S., Golubkova, E., Manu, Panok, L., Mamon, L., Reinitz, J., and Samsonova, M. (2013). Quantitative dynamics and increased variability of segmentation gene expression in the *Drosophila Krüppel* and *knirps* mutants. *Dev. Biol.*, 376(1):99–112.

Surkova, S., Kosman, D., Kozlov, K., Manu, Myasnikova, E., Samsonova, A. A., Spirov, A., Vanario-Alonso, C. E., Samsonova, M., and Reinitz, J. (2008). Characterization of the *Drosophila* segment determination morphome. *Dev. Biol.*, 313(2):844–862.

Tautz, D. (1988). Regulation of the *Drosophila* segmentation gene *hunchback* by two maternal morphogenetic centres. *Nature*, 332:281–284.

Wotton, K. R., Jiménez-Guri, E., Crombach, A., Cicin-Sain, D., and Jaeger, J. (2015a). High-resolution gap gene expression data from blastoderm embryos of the scuttle fly *Megaselia abdita*. *Scientific Data*, 2:150005.

Wotton, K. R., Jiménez-Guri, E., Crombach, A., Janssens, H., Alcaine-Colet, A., Steffen, L., Schmidt-Ott, U., and Jaeger, J. (2015b). Quantitative system drift compensates for altered maternal inputs to the gap gene network of the scuttle fly *Megaselia abdita*. *eLife*, 4:e04785.

Wotton, K. R., Jiménez-Guri, E., García Matheu, B., and Jaeger, J. (2014). A staging scheme for the development of the scuttle fly *Megaselia abdita*. *PLoS One*, 9(1):e84421.

Wotton, K. R., Jiménez-Guri, E., and Jaeger, J. (2015c). Maternal co-ordinate gene regulation and axis polarity in the scuttle fly *Megaselia abdita*. *PLoS Genetics*, 11(3):e1005042.